Measurement of Clear-Air Gradients and Turbulence Properties with Radar Wind Profilers

E. E. GOSSARD

Cooperative Institute for Research in Environmental Sciences, University of Colorado/NOAA, Environmental Technology Laboratory, Boulder, Colorado

D. E. WOLFE AND K. P. MORAN

NOAA/ERL/Environmental Technology Laboratory, Boulder, Colorado

R. A. PAULUS, K. D. ANDERSON, AND L. T. ROGERS

Naval Command, Control and Ocean Surveillance Center, San Diego, California

(Manuscript received 4 February 1997, in final form 29 May 1997)

ABSTRACT

An experiment comparing balloon and profiler observations was carried out to evaluate the capability of Doppler radar wind profilers to remotely measure useful meteorological quantities other than wind. The site chosen was in Southern California during a time of year when it offers a natural laboratory for investigating extreme contrasts in temperature and humidity. To evaluate the new capabilities, it was found that new and additional treatment of the radar data was necessary. For example, the adequacy of the usual radar wind observations obtained by editing the Doppler spectral moments was found to be very questionable for short-term observations, so the authors extended the editing to the raw spectra, and substantial improvement was found. The advantages of the redundancy in five-beam systems are investigated and are also found to be very necessary to obtain the accuracy needed. A technique for minimizing the variances of the differences of the four redundant pairs of radials is described. The resulting improved vertical velocity estimates substantially improve the agreement between radio acoustic sounding system (RASS) temperature retrievals and balloon-measured temperatures. The ability of the profilers to measure turbulence intensity was tested, and the accuracy of techniques using the spectral width to measure turbulent dissipation rate when complicated spectra are present is examined. Two different techniques for optimizing the calculation of spectral width are compared and the errors assessed. One technique integrates over the uncontaminated range of the chosen spectral peak and then extrapolates a Gaussian function to infinity. The other method uses the slope of the log least squares best fit of the uncontaminated points to a Gaussian function. Profiler-measured length scales of wind and scalar quantities are measured and compared. Profiles of radar-measured gradients of refractive index are compared with gradients measured by balloon. It is shown how gradients of humidity can be calculated to about the same accuracy as refractive-index gradients by combining the temperature gradients from RASS with the refractive-index gradient observations from the radar.

1. Introduction

Doppler radar wind profilers (e.g., Strauch et al. 1984) measure the radial velocity spectrum of target movement in the pulse volume. The first moment of the spectrum provides the mean radial velocity toward or away from the radar, thus giving the wind and wind shear profiles for which radar wind profilers were primarily designed. The horizontal and vertical wind components are defined as u, v, and w, respectively. When the radars are pointing vertically, the second moment (or width) of the spectrum contains information about the vertical component w of the turbulent velocity fluctuations, that is, the turbulent dissipation rate ϵ and structure parameter C_w^2 within the pulse volume. The theory and practice of using the spectral width to calculate the structure parameter of the turbulent velocity field (C_w^2 for the vertical velocity component w) was discussed by Gorelik and Mel'nichuk (1963), Srivastava and Atlas (1972), Frisch and Clifford (1974), Strauch and Merrem (1976), Labbitt (1981), Gossard et al. (1982), Gossard et al. (1990), Gossard and Strauch (1983), Hocking (1983, 1995), and Doviak and Zrnić (1984). In addition, from the zeroth moment of the spectrum [i.e., the radar-backscattered power from clear-air refractive-index tur-

Corresponding author address: Dr. Earl Gossard, NOAA/Environmental Technology Laboratory, R/E/ET4, 325 Broadway, Boulder, CO 80303-3328.
E-mail: egossard@etl.noaa.gov

bulence (RIT)], the structure parameter of turbulent refractive-index fluctuations C_ϕ^2 can be calculated, where ϕ denotes the potential refractive index.

Above the troposphere, most radar profiling has been done with VHF radars whose spectral second moments are not generally considered to be useful in the vertically pointing mode because of contamination of the backscatter by a specular component and because the beamwidths of these radars are usually large, therefore requiring large corrections for transverse winds. In addition, the pulse volumes become so large at great heights that it is unlikely that the inertial subrange can be considered to apply throughout the volume. However, off-vertical beams have recently been used by Nastrom and Eaton (1997) at the White Sands VHF facility, and the appropriate corrections for the broadening effect of wind shear for such off-zenith angles have been given by Nastrom (1997). Various assumptions are often made about the size of the outer scale and the existence and size of a buoyancy subrange scale over which the integration of the spectral energy density should be applied, and several adjustable constants are used, including a ''filling factor'' representing the percentage of the pulse volume that is assumed to be turbulent (vanZandt et al. 1978; Gage et al. 1980). Therefore, much of the work in the upper atmosphere has concentrated on combining radar-backscattered power with balloon-measured profiles of refractive index to deduce the turbulent dissipation rate. The various approaches have been reviewed by Fukao et al. (1994), Cohn (1995), and by Hocking (1995). In our experiment we use a 449-MHz radar with a 7.5° beamwidth and calculate turbulent dissipation rate profiles through a stratified atmosphere by both methods. We then compare the turbulence profiles.

Backscattered power from vertically pointing Doppler radars has long been recognized as providing an excellent representation of profiles of the gradient of radio refractive index in the atmosphere (e.g., Friend 1949; Saxton et al. 1964; Ottersten 1969; Richter 1969; Gossard et al. 1970; Chadwick and Gossard 1983; Gossard 1990). In Southern California the correlation between balloon-measured potential refractive-index gradient squared and the radar-measured refractive-index structure parameter was between 0.70 and 0.93 for all cases. Thus, the radar-backscattered power is inherently a very good predictor of refractive-index gradients aloft. For balloon-borne point sensors, compared with volume-measured radar sensing along a fixed direction, this correlation is impressively high because the different measurements are not collocated in either space or time. In fact, this correlation is higher than that found between the balloon-measured wind speeds and the radar-measured winds (0.40–0.79). As the profiles of specific humidity are virtual overlays of the profiles of potential refractive index in the lower atmosphere (except for scaling factors), conclusions about refractive-index profiling can be readily applied to humidity profiling. Therefore, radar-measured backscatter is already a very good predictor of humidity gradients, and the challenge is to generalize the empirical correlation with an improved description of the physical relationships between radar-measured quantities and other meteorological properties without degrading the correlation by introducing some noisy radar measurement (such as turbulence intensity, perhaps deduced from radar spectral second moments). We therefore examine radar computations of turbulence intensity in some detail and ask whether their incorporation improves or degrades the high correlations between humidity gradient and backscattered power found empirically.

This paper describes a data collection program carried out in Southern California during the season when large contrasts in air mass occur. During August through October, this area serves as a natural laboratory for the collection of data covering a wide range of conditions in a short time. The specific measurables of interest are mean wind, turbulence, Richardson number, radio refractive index, and humidity. The data were collected during September 1995. The collection site is shown in Fig. 1. Sample balloon soundings are shown in Figs. 2a,b and samples of the averaged Doppler spectra recorded by the radar are shown in Figs. 3 and 4. (Each spectrum shown is an average of 29 spectra.) Figures 3 and 4 were produced by the Profiler On-Line Program (POP) developed by NOAA's Aeronomy Laboratory.

2. Some theoretical background

The very close relationship between radar-backscattered power and gradients of radio refractive index has been observed for several decades (e.g., Friend 1949; Richter 1969), and it has often been suggested that this should offer a means of remotely sensing refractive-index gradients aloft. However, the relationships between mean gradients and the turbulence properties sensed by radars have proven to be elusive. For isotropic homogeneous turbulence in a horizontally homogeneous medium with vertical gradients of mean properties, Gossard et al. (1982) and Tatarskii (1971) showed that

$$\frac{C_\theta^2}{(d\theta_0/dz)^2}\frac{(du_0/dz)^2}{C_w^2} = \frac{B_\theta}{B_w}\left(\frac{K_m}{K_\theta} - \mathrm{Ri}\right)^{-1}, \tag{1a}$$

$$C_w^2 = B_w\epsilon^{2/3}, \tag{1b}$$

where θ_0 is the unperturbed potential temperature; C_θ^2 is the structure parameter of potential temperature; u_0 is the unperturbed horizontal wind; C_w^2 is the structure parameter of velocity along the vertical direction; $B_w = (4/3)B$, where B is a Kolmogorov constant equal to about 2.1; and B_θ is a similar constant equal to about 3.6. Here, K_m and K_θ are the eddy coefficients of momentum and temperature, respectively, and their ratio is the turbulent Prandtl number Pr. The gradient Richardson number is $\mathrm{Ri} = \omega_B^2/(du_0/dz)^2$, and $\omega_B = [(g/\theta_0)(d\theta_0/dz)]^{0.5}$ is the Väisälä–Brunt frequency, where g is gravitational acceleration. Some form of (1a) has been used by many

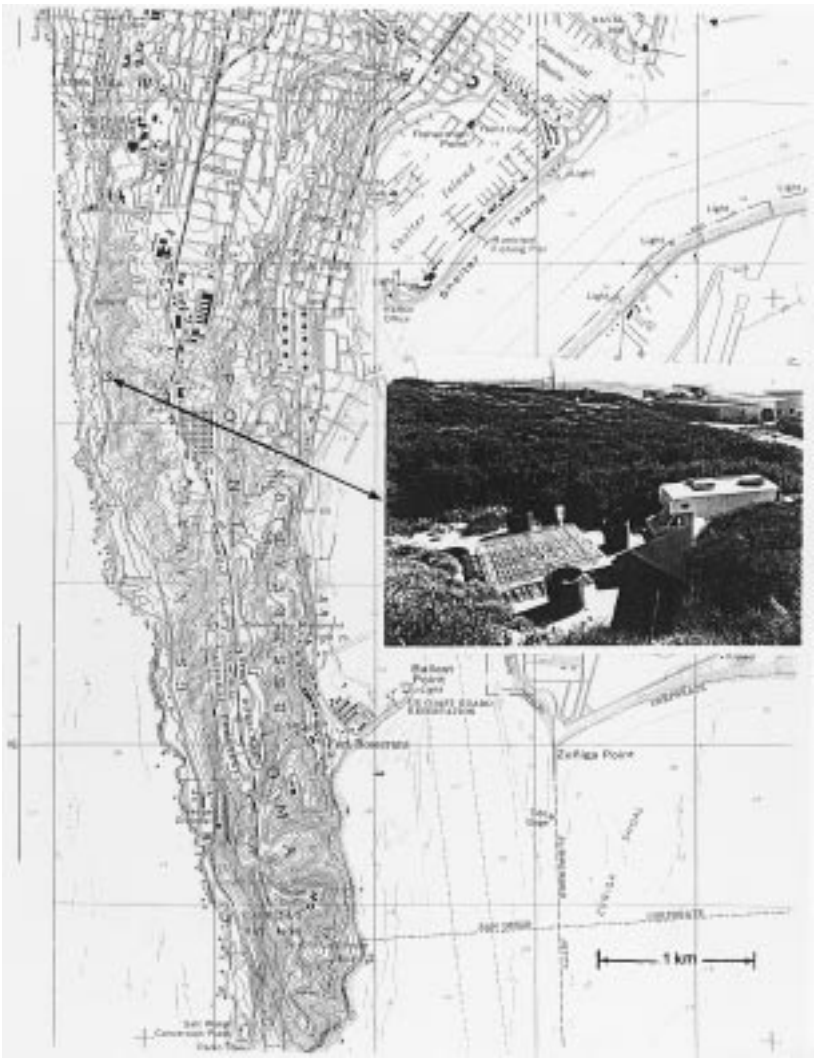

FIG. 1. Data collection site, Point Loma, San Diego, California. Insert: Photograph of radar phased-array antenna with RASS emitters in barrels.

researchers (e.g., vanZandt et al. 1978; Gage et al. 1980; Hocking 1983; Fukao et al. 1994; Warnock and vanZandt 1985) assuming various forms for Ri and outer scales (vanZandt et al. 1978). Furthermore, various adjustable constants are often used in parameterizing the right-hand side of (1a). Gossard et al. (1982) pointed out that the left side of (1a) can be expressed as a ratio of length scales to the 4/3 power; that is,

$$L_\theta^{4/3} = C_\theta^2 \left(\frac{d\theta_0}{dz}\right)^{-2} \tag{2a}$$

and

$$L_w^{4/3} = C_w^2 \left(\frac{du_0}{dz}\right)^{-2}, \tag{2b}$$

where

$$\left(\frac{du_0}{dz}\right)^2 = \left(\frac{du}{dz}\right)^2 + \left(\frac{dv}{dz}\right)^2, \tag{2c}$$

and u and v are the easterly and northerly components of the wind, respectively. The variables L_θ and L_w are variously referred to as ''outer scales'' or mixing lengths (e.g., Tatarskii 1971, 72). The length scales for all quantities that can be considered to be conserved and passive scalars (such as humidity in the absence of phase changes) will be given by equations similar to (2a). Obviously, the two lengths L_θ and L_w will not, in general, be the same. Furthermore, both will depend on stability and will be reduced under stable conditions because the eddy structure will be flattened by the work done against buoyancy in moving vertically. However, based on similarity arguments, Gossard et al. (1982) suggested that their *ratio may be approximately independent of sta-*

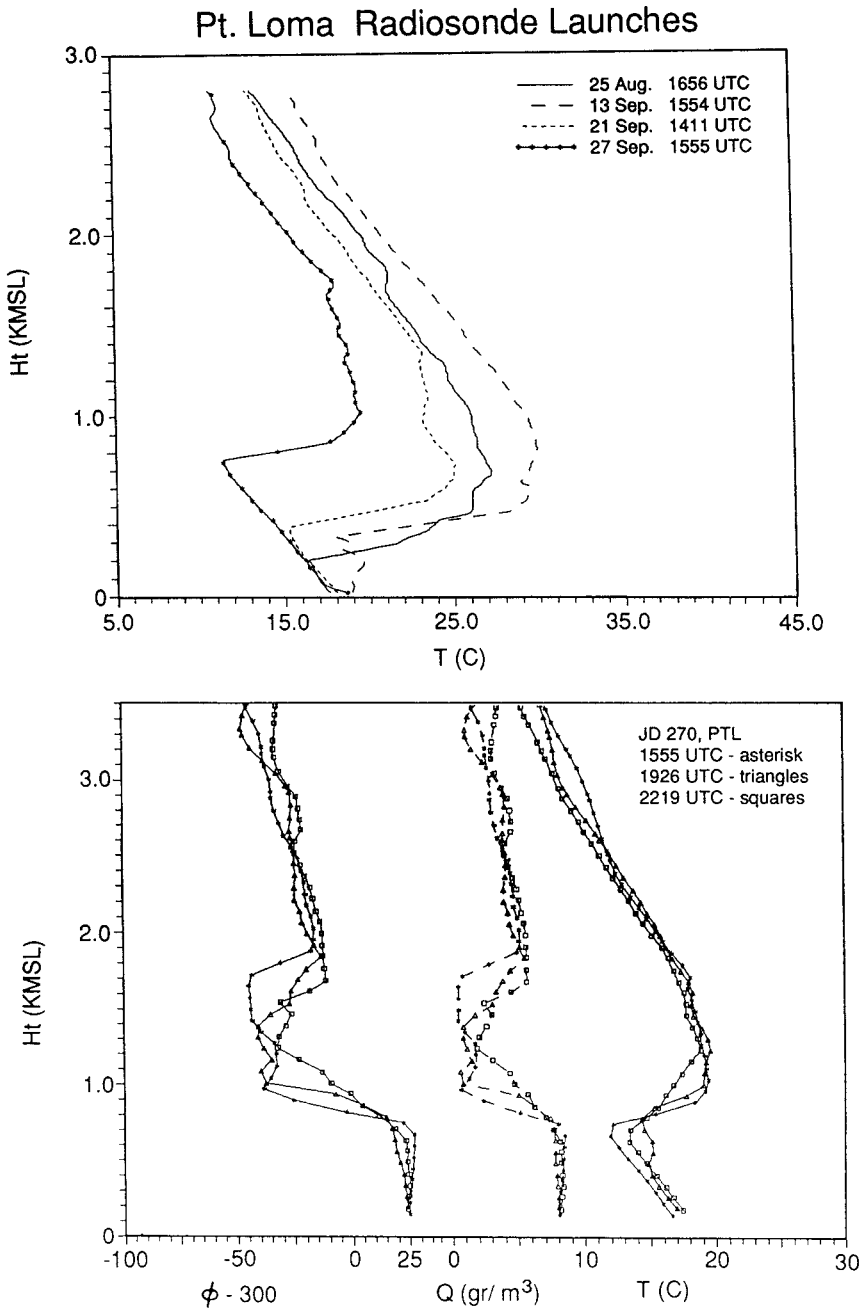

FIG. 2. (a) Profiles of temperature from balloon ascents at Point Loma during the period of observation. (b) Profiles of temperature, humidity, and refractive index at 1555, 1926, and 2219 UTC 27 September 1995 (JD 270).

bility because both heat and momentum are mixed by the same eddy ensemble. However, the effect of anisotropy within very stable layers is of concern. One primary goal of this study was the examination of the behavior of the various length scales in the very stratified environment often encountered in the San Diego area.

Equation (1a) applies only to a stably stratified atmosphere and assumes homogeneous, isotropic turbulence. Because C_w^2 is the convenient turbulence quantity measured by profilers, whereas shear is measured in the horizontal wind u, (1a) assumes that the redistribution of momentum among velocity components takes place fast enough that isotropy *essentially exists for those scales important to the experiment.*

From the same reasoning that led to (1a), it can be shown that similar relationships between structure parameters and gradients hold for other passive scalars

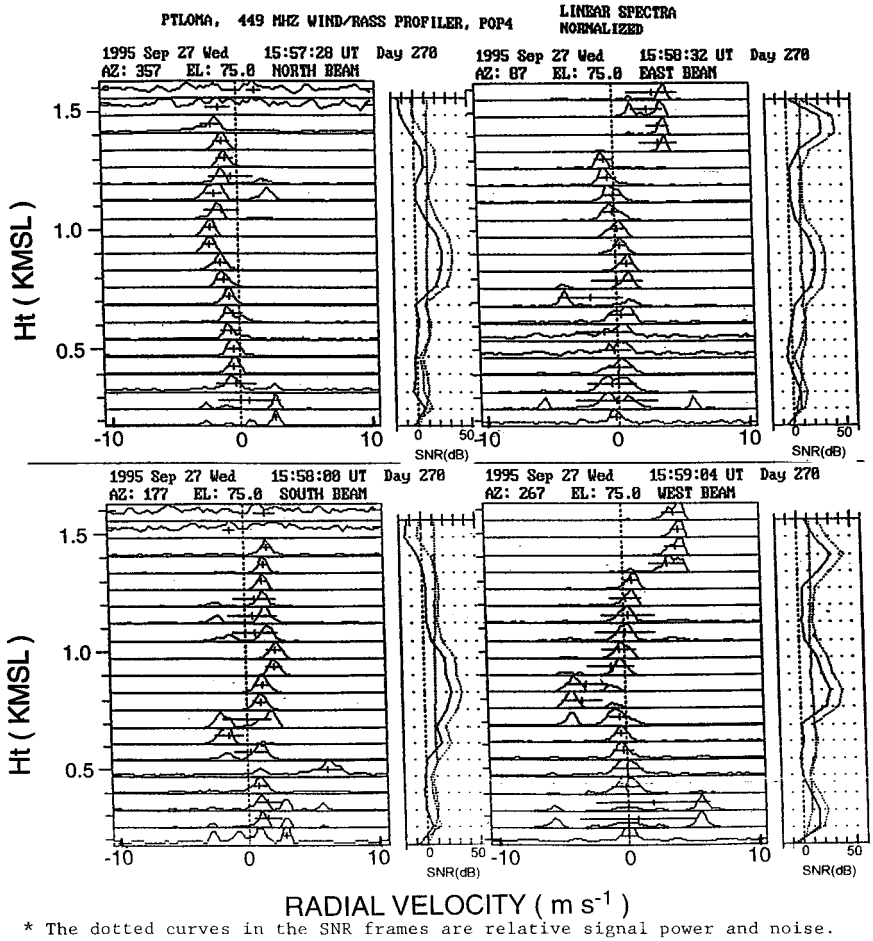

FIG. 3. Sample spectra output from the POP for the four beams that are 15° off vertical. Three complete radar cycles can be made during the time it takes for the balloon to rise to about 1800 m. This figure shows the first of three successive radar soundings during the 1555 UTC balloon sounding. The SNR frames show profiles of relative power in decibels (dashed) and signal-to-noise ratio in decibels (solid).

having the same spectral form. In particular, considerable effort has been devoted to justification of the conclusion that the potential refractivity ϕ has the same spectral form as the potential temperature θ and specific humidity q (Andreas 1987; Hill 1989). We use ϕ for potential refractive index, as introduced by Katz (1951), instead of M as is often seen, to avoid confusion with the ''modified index of refraction'' in radio propagation literature.

Gossard et al. (1984) reported measurements within a stable layer that rose across a suite of fast-response in situ sensors at 175-m altitude on a meteorological tower at Erie, Colorado. These measurements supported the equality $L_\theta = L_q = L_\phi \cong (1.3 \pm 0.1)L_w$. We note that these were point measurements, whereas the radar measurements of C_ϕ^2 and C_w^2 [see (2a) and (2b)] represent averages over the pulse volume of the radar in which the turbulence is assumed to be uniform and isotropic. The magnitude of C_ϕ^2 depends on the turbulence intensity at the turbulence Bragg scale (half the radar wavelength), which, at this frequency, virtually always lies within the inertial subrange. However, the calculated magnitude of C_w^2 requires the assumption that the inertial subrange extends to turbulence scales as large as the pulse volume. Therefore, in the present experiment, the radar scales defined by (2a) and (2b) in the zone of transition above the marine layer where the turbulence is likely to be anisotropic and where the turbulent outer scale is likely to be less than the size of the pulse volume were examined.

Other passive scalars such as potential refractive index ϕ can be substituted for potential temperature θ in (1a), so in this paper we usually replace θ with ϕ. The height gradient of refractivity can be written as

$$\left(\frac{d\phi_0}{dz}\right)^2 \simeq C\frac{C_\phi^2}{C_w^2}, \tag{3}$$

where

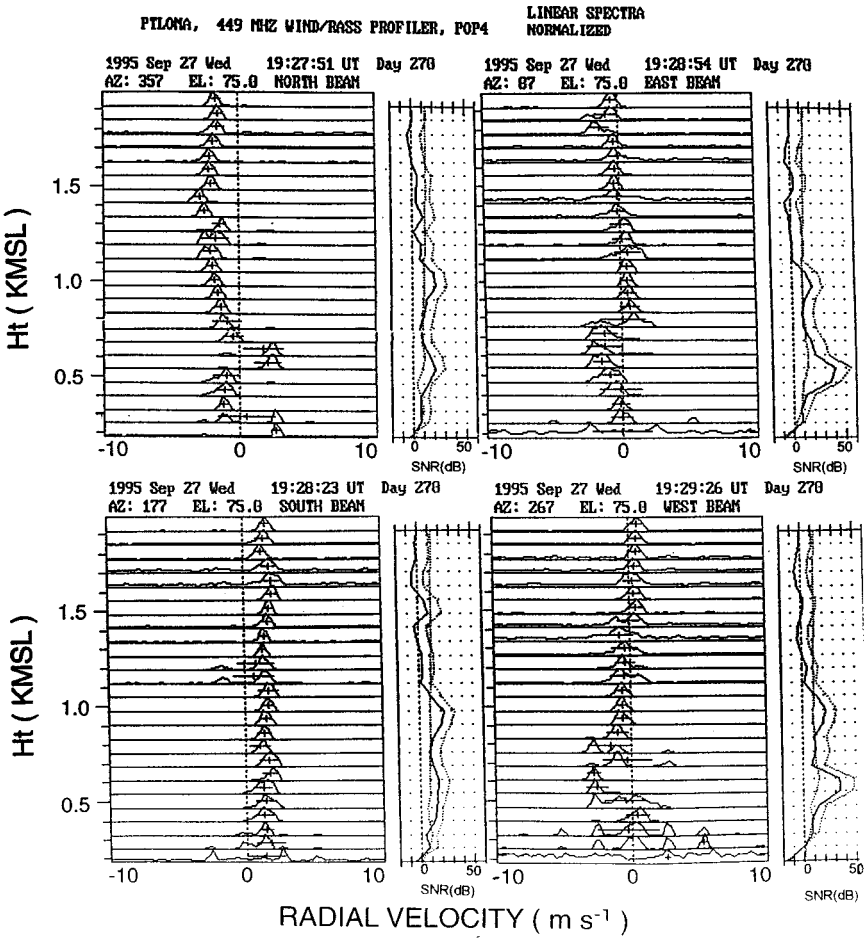

FIG. 4. Sample spectra output from the POP for the four beams at 15° off vertical. The second of three successive radar soundings during the balloon sounding launched at 1926 UTC is shown.

$$C = \left(\frac{L_w}{L_\phi}\right)^{4/3}\left(\frac{du_0}{dz}\right)^2 \equiv \left(\frac{B_w}{B_\phi}\right)(\mathrm{Pr} - \mathrm{Ri})\left(\frac{du_0}{dz}\right)^2. \quad (4)$$

Equation (4) shows good general agreement with experimental measurements of Pr and Ri summarized by Kondo et al. (1978). From similarity arguments, Gossard et al. (1982) suggested that L_w/L_ϕ should be a conservative quantity under steady conditions. It was also shown that

$$K_m = \frac{\epsilon}{\left(\frac{du_0}{dz}\right)^2(1 - \mathrm{Ri/Pr})}, \quad (5)$$

where ϵ is the turbulent dissipation rate if isotropic turbulence in an inertial subrange is assumed and (2c) is used in calculating shear. Equations in the form of (3) can be derived in a variety of ways: from the flux equation (Gossard and Frisch 1987; Gossard and Sengupta 1988), from the energy equation (Gage et al. 1980; Gossard et al. 1982), and from mixing length concepts (Tatarskii 1971). A conceptual derivation (Fig. A1) is illustrated in the appendix. However, as pointed out by Gossard et al. (1982), the form of (4) suggests a relationship between the Richardson number and the Prandtl number through the turbulence and shear properties measurable by radar. Thus, analysis of the behavior of the length scales may yield useful relationships for calculating the height gradient of refractive index from Doppler radar observations, if C_ϕ^2, du_0/dz, and C_w^2 can be provided by the zeroth, first, and second moments of the spectra of backscatter from Doppler wind profilers. An important goal of this experiment was to examine the length scales L_ϕ and L_w and the relative constancy of their ratio.

Since the time of the references listed above, radio acoustic sounding systems (RASSs), in which an acoustic source is added to the radar system, have been successfully demonstrated to measure accurate temperature profiles. Therefore, the Richardson number is now a fundamental measurable, and (1a) does not require the very restricting assumptions about Ri (e.g., Ri = 0.25)

often made in the earlier work. (Note that because of the poor height resolution, the Ri measured by the radars are ''bulk'' quantities and are not suitable for detection of thin lamina.) When (1a) is expressed in terms of potential refractive index instead of potential temperature, it permits the turbulent Prandtl number (K_m/K_θ) to be deduced if the radar sounding is accompanied by a balloon sounding (as in our experiment) of the profile of refractive index.

The quantities w and ϕ are henceforth defined to be the perturbation quantities; the unperturbed quantities will have zero subscripts. [We note here that $\overline{w^2}/\overline{\phi^2} = C_w^2/C_\phi^2$ if $\overline{\phi^2} = f(L)C_\phi^2$ and $\overline{w^2} = f(L)C_w^2$, as, for example, in the inertial subrange, where $f(L) = L^{2/3}$ and L is a generic size scale of turbulence.]

Finally, if temperature profiles are available from RASS, we shall see that profiles of the humidity gradient dq_0/dz can be found. For meteorological purposes, profiles of gradients such as provided by (3) are not as interesting as profiles of mean quantities such as temperature and humidity. Simply integrating (3) to obtain ϕ_0 is usually not practical because of the sign ambiguity and because the important lower levels of profiler soundings are usually inaccurate due to ground clutter, aircraft reflections (near airports), birds, and insects. However, if algorithms used in radiometric retrieval are constrained by radar-provided gradients and thicknesses at known altitudes, detailed structure of the mean quantities can, in principle, be retrieved (Stankov et al. 1996). Alternatively, the radar observations may be assimilated into models to provide detailed structure.

3. The experiment

The primary goal of the experiment was to compare profiler results with the in situ data collected by balloon-borne sensors launched at the radar site. [The launch site was actually about 750 m distant. The balloon reached the typical maximum height of the RASS soundings (1.6 km) in 10 min. Therefore, for a wind of 5 m s^{-1}, the balloon drifted 3 km from the radar site during the sounding.] Quantities such as wind, gradients of refractive index and humidity, temperature, and Richardson number are readily compared. However, other radar measurables such as turbulence intensity, outer scale, and Kolmogorov microscale cannot be measured with ordinary balloon sensors. The qualitative reasonableness of the turbulence profile through the transition zone between the turbulent marine boundary layer and the essentially nonturbulent region above provides a useful qualitative indication of the sensitivity of the method. The balloon traversed the lowest 2 km in about 10 min, corresponding to three full cycles of the profiler. The balloon soundings were made using a Väisälä MARWIN system with an Omega receiver to provide location and winds.

The radar observations were collected with a 449-MHz wind profiling radar built as an experimental prototype by the System Demonstration and Integration Division of the Environmental Technology Laboratory. Its characteristics are listed in Table 1. The profiler was located at the base of an erosion gully on the west side of Point Loma, 33 m above sea level. The walls of this gully helped shield the radar from much of the ''noise'' from local unwanted targets and emissions (see Fig. 1).

TABLE 1. Characteristics of the 449-MHz wind profiler radar.

Characteristics	Value
Frequency	449 MHz
Bandwidth	2 MHz
Peak power	900 W
Antenna aperture	4.25 m × 4.25 m
One-way beamwidth	7.5°
Pulse width	0.5 μs
Gate spacing	0.5 μs
Pulse repetition period	35 μs (selectable)
Number of pulses averaged	440
Number of spectra averaged	29
Folding velocity	10.8 m s^{-1}
Spectral resolution	0.338 m s^{-1}
First height	150 m
Height spacing (ΔR)	75 m
Number of heights	50

The profiler uses a phased-array antenna that provides a vertical beam and four off-vertical beams with zenith angles of 15°. These beams were oriented at north, south, east, and west azimuths (357°, 177°, 87°, and 267°). The profiler cycles through the five beams in 3 min 18 s, so the dwell time on each beam is about 40 s. Twenty-nine spectra were calculated and averaged using 64-point FFTs of 440-pulse time series.

4. The data reduction and analysis

As noted above, it was found to be very important to edit the radar spectra rather than use the spectral moments calculated in real time by the POP software. The standard technique of editing moments by consensus is not applicable to this experiment because only those radar soundings collected during the balloon traverse are of interest. The balloon took about 10 min to rise through the height range where RASS signals were above noise level (1.5 km). During this 10-min interval, the radar cycled through three five-beam sequences plus RASS, and the average of those three cycles was compared with the balloon data.

Figures 3 and 4 show examples of spectra collected by the radar during the balloon traverse starting at 1555 UTC. It is evident that the lowest range gates are severely contaminated by extraneous targets and local radio frequency emissions. Many of the unwanted spectral peaks result from aircraft, ships, and cars appearing in the antenna sidelobes. Some resemble individual birds such as sea gulls that are common in the vicinity. The lowest four or five gates are usually severely contaminated. Consequently, the data that we analyzed in detail for this study were collected on those days when the

atmospheric layering occurred above gate 5 (about 550 m). Figure 2a shows that the stable layers usually lay within the region of largest clutter contamination of the spectra during much of the experimental period. The date 27 September 1995 [Julian day (JD) 270] was chosen for detailed analysis because the inversion layer is above the main clutter. Three balloon soundings were made on JD 270 with launches at 1555, 1926, and 2219 UTC. The temperature, humidity, and refractive-index profiles are shown in Fig. 2b.

It is clear from Figs. 3 and 4 that extraction of the correct wind profiles from these data is fundamentally difficult because of the many extraneous spectral peaks from which the desired atmospheric signal must be selected. The choice by the POP is shown by the (+) signs on the individual spectra. Very often, they do not correspond with selections by human judgment. We see from equations such as (1)–(3) that accurate winds are of fundamental importance if higher-order quantities are to be extracted from the data. Accurate winds are also absolutely fundamental in the calculation of shears (as required, e.g., by the Richardson number) and are imperative in correcting the spectral width needed to get the turbulent dissipation rate. We believe that many efforts to extract turbulence information from the second moment (spread) of the Doppler spectrum have failed because of inadequate accuracy of the winds transverse to the vertical beam and because of very erroneous spectral widths found by the POP (e.g., see the second moments in the lower gates of Figs. 3 and 4, as shown by the horizontal solid lines about the average on each spectrum). Therefore, a five-beam profiler system was used that provided useful redundancy.

Clearly, in an ideal homogeneous atmosphere, the east and west radial wind measurements should lead to the same east–west wind component, and the north and south components should give the same north–south component. However, the real atmosphere is not homogeneous. Furthermore, the vertical wind component needed in the calculation of horizontal projections of the measured radial velocities is not very accurate because of ground and sea clutter and the filtering used to suppress it. Therefore, a technique of minimizing the variance of the differences in the calculated horizontal components from east and west, and from north and south radials by varying vertical velocity, will be described. This greatly reduced the spread of the redundant profiles and produced believable vertical velocities that also improved the Doppler correction of the RASS temperatures when compared to balloon virtual temperatures. Averages of the components of the four redundant profiles were then used to calculate the speed, direction, and shear.

5. Refractive index of microwave frequencies

For microwave frequencies, electromagnetic propagation through the atmosphere is essentially nondispersive. The refractive index n is therefore independent of wavelength and is related to constituents of the air (e.g., Bean and Dutton 1966).

For the interpretation of clear-air radar backscatter, we are mainly concerned with turbulence processes in which both heat and moisture are conserved. We usually assume no change of state (condensation or evaporation) and assume that parcel movements occur quickly enough so that temperature changes are essentially adiabatic, that is, the parcel does not lose or gain heat by some process such as radiative transfer. For these problems, it is very convenient to use potential refractivity $\tilde{\phi}$ (analogous to potential temperature), defined by

$$\tilde{\phi} = \frac{77.6p_r}{\tilde{\theta}}\left(1 + \frac{7.73\tilde{Q}}{\tilde{\theta}}\right), \tag{6}$$

where Q is specific humidity (g kg^{-1}) (i.e., $Q = q \times 10^3$), $\tilde{\theta}$ is potential temperature (K) for dry air given by

$$\tilde{\theta} = \tilde{T}\left(\frac{p_r}{\tilde{p}}\right)^{0.286},$$

and p_r is some reference pressure level often chosen to be 1000 mb. The tilde is used for the total quantity to distinguish it from the unsubscripted perturbation component and the zero-subscripted mean used later. We see that $\tilde{\phi}$ is the N value of a parcel moved from its ambient level to the reference level adiabatically without loss or gain of moisture. The conserved property, potential refractivity $\tilde{\phi}$, is the convenient atmospheric parameter for most atmospheric science purposes, but, of course, the radar senses n.

6. Techniques for extracting meteorological quantities from radar data

a. Calculating C_ϕ^2 from backscattered power (zero moment of Doppler spectrum)

Equations such as (3) require that C_ϕ^2 and C_w^2 be calculated from radar data. Calculation of C_ϕ^2 from the radar requires true, calibrated received power P_r. The radar equation for atmospheric ''Bragg'' backscatter is given in many standard texts (e.g., Atlas 1964; Battan 1973; Gossard and Strauch 1983; Doviak and Zrnić 1984). For present purposes, we neglect attenuation in the intervening medium between scatterer and radar and consider only backscatter. Then, designating radar reflectivity as η, the received power assuming a Gaussian beam antenna is (e.g., Battan 1973)

$$P_r = \pi P_t A_e \Delta R \eta / [128 R^2 \ln(2)], \tag{7}$$

where P_t is the transmitted power, A_e is the effective antenna aperture, ΔR is the range resolution (equal to $c\tau/2$, where τ is the pulse duration and c is the velocity of light), and R is range to the target. Thus, (7) may be

used to find η. For general Bragg scatter at an angle θ from the direction of the incident wave,

$$\eta = -2\pi k^4[E_n(\kappa)/\kappa^2] \sin^2\chi. \tag{8}$$

Here, $k = 2\pi/\lambda$, where λ is radar wavelength, and $\kappa = 2k \sin(\theta/2)$. For backscatter, $\theta = \pi$, so $\kappa = 2k$ and $E(\kappa) = E(k)$ is the power spectrum of the potential refractive-index (ϕ) fluctuations, given by $E_n(k) = -k[\partial S(k)/\partial k]$ (Corrsin 1951), where $S(k)$ is the one-dimensional spectrum along a line through a medium whose turbulence is isotropic and homogeneous; χ is the angle between the polarization of the incident wave and the scattering direction ($\chi = 90°$ for backscatter). Thus, the important scattering scale in the problem is $2\pi/\kappa = \pi/k = \lambda/2$, which defines the important backscattering scale in the turbulence ensemble. It has come to be called the Bragg scale by rough analogy with Bragg's results for scatter in crystal lattices. Therefore, radars can remotely sense the refractive-index variance density of the spectral component corresponding to the Bragg scale. It has often been assumed that the refractive-index spectrum in the neighborhood of the Bragg scale has the inertial convective subrange (ICS) form and, therefore, that the radar refractive-index spectrum follows the same $k^{-5/3}$ law that governs potential temperature (for adiabatic fluctuations) and specific humidity; a great deal of work has gone into demonstrating that this is essentially true (Hill 1978; Andreas 1987). [It depends on the nature of the temperature–humidity correlation, which has been examined by Gossard (1960), Wyngaard et al. (1978), and Priestley and Hill (1985).] If the refractive index takes the ICS form, the radar reflectivity for backscatter is given by (Atlas et al. 1966; Ottersten 1969; Muschinski 1997)

$$\eta \approx 0.38C_\phi^2\lambda^{-1/3}, \tag{9}$$

where C_ϕ^2 is the turbulence structure parameter for radar refractive index. (In this report we use the potential refractive index ϕ rather than N and the potential refractive-index structure function C_ϕ^2 instead of C_N^2.) Thus, from measurements of backscattered power from RIT, the refractive-index structure parameter C_ϕ^2 (or C_N^2) can be deduced. Insects, clouds, and birds can cause severe contamination of this measurement and must be carefully assessed.

b. Calculating the velocity structure parameter from spectral width

There have been many attempts to use spectral width from profilers to measure turbulence intensity without much success (e.g., see Gossard et al. 1990; Cohn 1995). Reference to the spectra in Figs. 3 and 4 in which the spectral width is represented by the horizontal line through the first moment (+) at each gate makes it clear why previous efforts have met with so little success. Contamination by unwanted targets is especially detrimental to second-moment calculations.

The use of the Doppler spectral width as a measure of mechanical turbulence intensity depends critically on the finite size of the pulse volume of the radar. If all scattering elements within the volume were moving toward or away from the radar with the same radial velocity V_r, the backscattered signal would simply be Doppler-shifted in frequency by $2V_r/\lambda$, where λ is wavelength and the spectrum of the signal would have zero width. However, if the scattering elements within the pulse volume are moving with different radial velocities, the spectrum of the backscattered signal will be spread about the mean V_r according to the spread in velocity of the scatterers. For isotropic turbulence, the velocity half-variance is given by

$$\sigma^2 = \int_0^\infty E(k)\, dk, \tag{10}$$

where, within a fully developed ICS, the kinetic energy density is

$$E(k) = \alpha\epsilon^{2/3}k^{-5/3}; \tag{11}$$

here, $\alpha \simeq 1.6$ is a Kolmogorov constant, and k is wavenumber. Thus, ϵ is directly related to the total velocity half-variance. However, the radar senses only the variance within the limited pulse volume of the radar. Therefore, observing radial velocity (say, w) with a radar whose antenna has finite angular half-beamwidth α and whose pulse length is ΔR essentially imposes a low-pass filter on the spatial structure of the velocity field being carried past the radar by the wind. We use the spectral broadening to calculate turbulent dissipation rate and structure functions. For isotropic, homogeneous turbulence, the spectral energy density tensor is given by (e.g., Lumley and Panofsky 1964)

$$\phi_{zz}(\underline{k}) = \frac{E(k)}{4\pi k^2}\left(1 - \frac{k_z^2}{k^2}\right) \tag{12}$$

for the z component of velocity along the z direction. Here, $E(k)$ is the kinetic energy density spectrum given by (11), and $k^2 = k_x^2 + k_y^2 + k_z^2$. Frisch and Clifford (1974) integrated (12), assuming Gaussian beamwidth and pulse shape (e.g., see Gossard and Strauch 1983, appendix D). The Frisch–Clifford method gives

$$\epsilon = \frac{1}{\delta}\left[\frac{\sigma_{Vw}^2}{\frac{3}{2}\Gamma\left(\frac{5}{3}\right)\alpha\gamma^2}\right]^{3/2}, \tag{13}$$

where σ_{Vw}^2 is the variance in w within the pulse volume V, Γ is the gamma function,

TABLE 2. Definitions of relationships between radar constants and physical quantities (see Table 1). (PRP: pulse repetition period; NPA: number of pulses averaged; NSA: number of spectra averaged; FFT: fast Fourier transform; gt: gate number.)

Parameter	Relationship
Folding velocity	$W_f = \lambda/[4\ (\mathrm{PRP})(\mathrm{NPA})] = 10.8\ \mathrm{m\ s^{-1}}$
Spectral resolution	$\Delta W = W_f/32$ for a 64-point FFT
Dwell time	$t_D = (\mathrm{NSA})\ [64\ (\mathrm{PRP})(\mathrm{NPA}) + t_0]$ for a 64-point FFT and a processing time of t_0 seconds
Range	$R = 150 + \Delta R \times (\mathrm{gt} - 1)$

$$\left.\begin{aligned} \delta &= a \\ \gamma^2 &= 1 - \frac{h}{15} - \frac{h^2}{105} - \cdots \\ h &= 1 - \left(\frac{b}{a}\right)^2 \end{aligned}\right\} \quad \text{for } b \le a,$$

and

$$\left.\begin{aligned} \delta &= b \\ \gamma^2 &= 1 - \frac{4h}{15} - \frac{8h^2}{105} - \cdots \\ h &= 1 - \left(\frac{a}{b}\right)^2 \end{aligned}\right\} \quad \text{for } b > a,$$

where a is half the diameter of the (circular) beam cross section and b is the half-length of the pulse. The γ^2 are confluent hypergeometric expansions introduced by Labbitt (1981) for the Frisch–Clifford integral.

c. Corrections for other factors that can broaden the radar-observed spectrum

1) DWELL TIME

Another important consideration in spectral broadening by turbulence is the temporal variability of the mean wind as the turbulence is advected through the pulse volume. The width described by (13) is the width of one realization of the spectrum from a 440-pulse series returning from a turbulent pulse volume. Table 1 shows that 29 spectra are averaged, leading to a dwell time (see Table 2) of 40 s. Spectral scales larger than the pulse volume Doppler-shift each spectral realization by an amount corresponding to the velocity of that spectral scale, so that the spectra are randomly moved about on the velocity axis and the spectral width of the average spectrum is broadened. The largest scale contributing to the broadening will be the product of the mean transverse wind and the dwell time. For our system, a mean wind of 10 m s^{-1} corresponds to a scale of 400 m, which is almost three times the width of our pulse volume at a height of 1 km. Therefore, the mean spectrum produced by the radar is substantially broadened when compared with that from one spectral realization. Because the observed spectra will be broadened by scales larger than the pulse volume, an assumption must be made about the form of the spectrum at the larger scales.

Let the variance contributed by the instantaneous spatial variability of w within the pulse volume be [from (13)]

$$\sigma_{\bar{V}w}^2 = \frac{3}{2}\alpha\delta^{2/3}\epsilon^{2/3}\Gamma\left(\frac{5}{3}\right)\gamma^2,$$

where δ and γ depend on the larger dimension (a or b) of the pulse volume [see (13)]. Let the additional variance, due to the length of the temporal record, be given by the one-dimensional spectrum E_1,

$$\sigma_T^2 = \int_{k_0}^{k_a} E_1(k_x)\, dk_x, \tag{14}$$

where $k_0 = 2\pi/(V_T t_D)$ and $k_a = \pi/a$. [*Note that "a" is the half-scale (beamwidth) size of the pulse volume.*] Thus, the total variance contributing to the spectral line broadening, measured by the radar, is

$$\sigma_w^2 = \sigma_{\bar{V}w}^2 + \sigma_T^2.$$

Letting $E_1(k_x) = \alpha_1\epsilon^{2/3}k_x^{-5/3}$, where $\alpha_1 \approx 0.5$ is a Kolmogorov constant, and integrating (14), we find

$$\sigma_w^2 = \sigma_{\bar{V}w}^2 + \frac{3}{2}\alpha_1\left(\frac{\epsilon}{2\pi}\right)^{2/3}[(V_T t_D)^{2/3} - (2a)^{2/3}] \tag{15}$$

as the variance causing the radar-sensed line broadening, and thus

$$\epsilon^{-2/3} = \frac{1}{\sigma_w^2}\alpha\left\{\frac{3}{2}\Gamma\left(\frac{5}{3}\right)\delta^{2/3}\gamma^2 + \frac{3}{2}\frac{\alpha_1}{\alpha}(\pi)^{-2/3} \times [(V_T t_D)^{2/3} - (2a)^{2/3}]\right\}. \tag{16}$$

Therefore, (13) becomes (Gossard et al. 1990)

$$\epsilon = \frac{1}{\delta}\left[\frac{\sigma_w^2}{\alpha\left\{\frac{3}{2}\Gamma\left(\frac{5}{3}\right)\gamma^2 + \frac{3}{2}\frac{\alpha_1}{\alpha}\left(\frac{2a}{\pi\delta}\right)^{2/3}\left[\left(\frac{V_T t_D}{2a}\right)^{2/3} - 1\right]\right\}}\right]^{3/2}, \tag{17}$$

where α, δ, a, b, and γ^2 have the same meanings as in (13) and where σ_w^2 is the total second-moment variance of the RIT spectrum measured by the radar. To prevent the contribution from dwell time being negative, the right-hand term in braces in the denominator is ignored unless $V_T t_D > 2\delta$. Here, C_w^2 is found from $C_w^2 = \beta_w\epsilon^{2/3}$, where $\beta_w = (4/3)B$ and B is a Kolmogorov constant approximately equal to 2.1. Having ϵ and C_w^2, an inner scale ℓ_0 can be calculated from

$$\ell_0 = \left(\frac{\nu^3}{\epsilon}\right)^{1/4}, \tag{18}$$

where ν is kinematic viscosity (Gossard et al. 1984). This inner scale may be compared with (2b), which gives a kind of outer scale for vertical mixing.

2) Beamwidth and wind shear

Several factors other than turbulence can cause the measured second moment of the Doppler spectrum in clear air to be broader than it would be if the turbulence contribution were the only factor, and these require correction in real radar systems.

If there is shear in the mean wind, the speed and direction of the mean wind may vary significantly within the pulse volume, causing broadening of the Doppler spectrum. The important effect is the radial variation in the radial component of the mean wind. Thus, vertical shear in the horizontal wind causes no spectral broadening for a vertical beam, whereas the shear effect is maximum for transverse (vertical) shear in the wind component parallel to a horizontal beam. This correction has been addressed by Nastrom (1997), who has used spectral broadening in the off-vertical beams of a VHF radar profiler to deduce eddy diffusion and dissipation in the upper atmosphere (Nastrom and Eaton 1997).

Even if the beam is vertical, as is the case with one beam of most wind profilers, there is some broadening of the spectrum due to the finite beamwidth of the antenna even when there is no shear. That is, the edges of the beam have a radial component of the mean horizontal wind toward and away from the radar. This is important for most profiler systems because their antennas have fairly broad beams. The correction is given by

$$\sigma^2 = V_T^2\theta_a^2/(2\ \ln 4), \tag{19a}$$

where V_T is the component of the mean wind transverse to the beam.

There is a potential contribution due to radial shear in the mean radial wind. However, for a vertical antenna, this requires a substantial height variation in the mean vertical velocity, which should be negligible. Sirmans and Doviak (1973) gave this correction as

$$\sigma^2 = (\beta_R \Delta R)^2/12, \tag{19b}$$

where β_R is the radial shear in the radial component of the mean wind and ΔR is range cell length.

For scanning radars, there is also a broadening effect due to the motion of the antenna, but this is irrelevant to most profilers. The general case, when the spectral broadening contributions are not completely independent, has been recently described by Nastrom (1997). We see that most of the nonturbulent broadening contributions do not affect the vertical beam. However, the finite beamwidth contribution requires a substantial correction to the measured widths of our spectra.

d. Techniques used for extracting second-moment information in noisy environments

Wind and shear information is obtained from the first moment of the Doppler spectrum. Wind is the principal output of the POP program. Very large errors are routinely present in the data when artificial targets and heavy clutter exist in the radar environment. In the present study, editing of the moment data was found to be unsatisfactory, so the raw spectra were examined and edited. When there were multiple overlapping peaks in the spectra, a human choice of peak sometimes had to be made based on coherence of the patterns and time and height persistency. Bounds were also determined at which the contribution from a selected peak became contaminated by contributions from adjacent target peaks. The three moments were then calculated for the selected peak.

The second-moment calculations of spectral width, needed to calculate ϵ, were done in two ways for comparison and error assessment. In method 1 the integrations were carried out over the part of the selected spectral peak between the uncontaminated bounds. In method 2 a Gaussian form of the spectrum was assumed to be appropriate for atmospheric backscatter (Batchelor 1953; Labbitt 1981), and a regression fit to a Gaussian shape was then found from the uncontaminated points. The slope of the regression line on a plot of $\log C_n^2$ versus w^2 was then used to determine spectral width. Thus, if the spectral density of C_ϕ^2 is given by the Gaussian function

$$S = S_0 \exp[-(w^2/2\sigma_w^2)], \tag{20}$$

it can be written logarithmically as an equation linear in w^2; that is,

$$\log S = \log S_0 - [(2)(2.3026)\sigma_w^2]^{-1} w^2, \tag{21}$$

where σ_w^2 is the variance and the spectral width is here defined as $2\sigma_w$. Therefore, the slope of the regression line of (21) on a log plot is proportional to σ_w^{-2}. Method 2 has been used by Gossard et al. (1997) to determine the broadening of radar-measured cloud drop-size spectra by atmospheric turbulence. Finally, the calculated spectral width was corrected for broadening by the finite antenna beamwidth and dwell time, as described above.

Calculations of resulting profiles of ϵ through the strong temperature inversion on JD 270 are shown in Fig. 5, where the dashed profile is calculated by method 1 and the solid profile is calculated by method 2.

The profile of heavy dashes in Fig. 5 shows ϵ found by solving (3) for C_w^2 using the balloon-measured profile of $d\phi/dz$ and by assuming the ratio L_w/L_ϕ to be unity. Using (1a), ϵ is then easily calculated. This is basically the ''power method'' introduced by Gage et al. (1980). Above the mixed layer, where (1) should apply, the profiles of ϵ calculated from C_ϕ^2 somewhat resemble the profiles found from the spectral width, but the magnitudes are considerably smaller. This may be because we

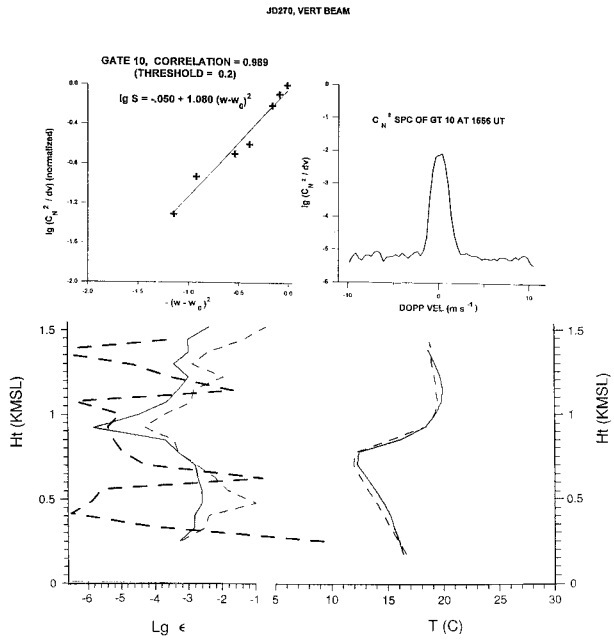

FIG. 5. Balloon and RASS temperature profiles and profiles of ϵ calculated by the three techniques (solid, dashed, and heavy dashed) described in text. The top left frame shows the regression fit of the spectrum S (top right) of C_N^2 density at gate 10 at 1556 UTC to a Gaussian function. The correlation coefficient is 0.98, indicating that a Gaussian function fits the spectrum well. The inverse slope of the regression line (top left) is proportional to the square of spectral width (variance) used to calculate ϵ (solid curve) [see (21)]. The dashed profile was found from the second-moment integral, which can be sensitive to its bounds; the anomaly at 0.5 km results from a too-liberal choice of bounds. The heavy-dashed profile is that deduced from (3) using the balloon sounding of $d\phi/dz$ and the radar sounding of C_ϕ^2.

have ignored the filling factor proposed by vanZandt et al. (1978) and have used the radar-measured values of C_ϕ^2. It is probably related to our assumption of a ratio of length scales of unity, which will be found to contradict our length scale computations in later sections. Tower measurements of ϵ tend to lie between 10^{-4} and 10^{-3}.

The balloon was launched at 1555 UTC and took about 10 min to rise through the height range penetrated by the RASS system. During that period, the radar cycled through three complete five-beam sequences. The curves in Fig. 5 are the average ϵ measured for the three cycles. Method 2 tends to yield smaller values of spectral width than method 1. It is unaffected by noise level and choice of bounds on the spectral peak, and it produces a correlation coefficient that is a measure of ''goodness of fit.'' It is more objective, and we conclude it is usually the preferable method. A sample of the regression fit for gate 10 is shown in the top frames of Fig. 5. The correlation coefficient for this case is 0.98, suggesting adequacy of the Gaussian to represent the spectral shape. As the methods 1 and 2 are nearly independent, their difference provides an estimate of the error in the spectral width technique for measuring turbulence intensity. The anomaly at 0.5 km found by method 1 (dashed line) is a result of a too-liberal choice of bounds at that height. We see that the turbulence is extremely weak in the upper part of the stable layer (see Fig. 5), and we will see that the outer scale becomes so small that the inertial subrange approximations inherent in some of the above derivations become questionable. Isotropy and homogeneity assumptions are also very likely to fail to some degree.

e. Techniques for optimizing wind profiles and shear (minimizing the variance of the differences)

As illustrated by Figs. 3 and 4, calculations of winds from individual profiles of first moments are very erratic, and the use of the POP outputs to calculate wind for direct comparison with balloon-measured wind profiles were quickly rejected because time and height consensuses were impractical for the time frame of the balloon ascent (about 10 min). We therefore edited the spectra as described above rather than editing the moments as is conventionally done. We also had a five-beam system that provided redundancy in the wind estimates (i.e., four off-vertical beams provide four profiles of wind speed and direction). Under homogeneous, steady conditions, oppositely directed wind radials should yield identical horizontal components of wind. However, the radial components are not equal and opposite unless the vertical velocity is zero, and the vertical beam is inherently noisy because of clutter and the various techniques for its removal. We therefore used vertical velocity to minimize the variance of the differences (MVD) between the horizontal components calculated from the four radials. That vertical velocity was then used to calculate wind speed and direction. This technique substantially decreases the scatter between the redundant wind profiles calculated from the four orthogonal pairs of radials, as shown by the example in Fig. 6, and leaves a residual scatter that we believe to be due primarily to true spatial inhomogeneity. It had the unexpected bonus of improving the RASS estimates of temperature.

f. Corrections of RASS temperature (importance of MVD)

The RASS systems have been described elsewhere (e.g., Peters et al. 1983; May et al. 1989), so we will not describe them here. However, we note that the radar measurement of acoustic velocity yields a virtual, apparent temperature that must be corrected for humidity and for the vertical velocity of the atmosphere in which the acoustic wave is embedded. In our experiment, we had observed humidity measured by a collocated balloon profile at the same time as the radar observations, so the humidity correction may be considered to be accurate. However, the vertical velocity profile was

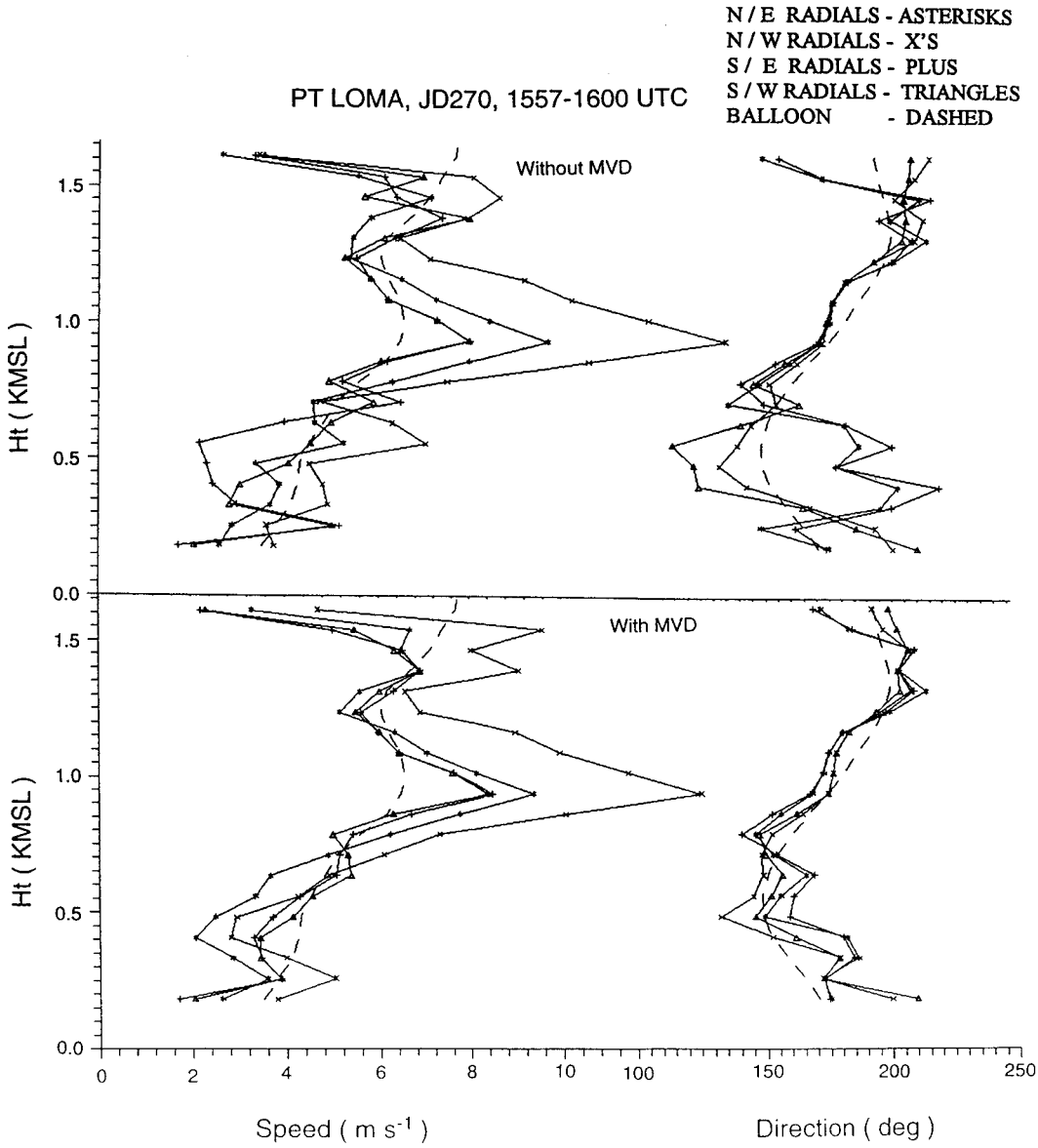

FIG. 6. Sample illustrating the use of the MVD technique (see text) to improve the wind profile estimates. The top frames do not have the MVD applied. The lower frames are the same data with MVD applied.

found to be sometimes noisy and inaccurate. We therefore used the vertical velocity yielded by the MVD method described above to correct the RASS temperature for the Doppler effect of vertical motion in the medium.

Figure 7 illustrates the importance of the correction. The left-hand frame shows the three temperature profiles corrected using the vertical velocities provided by the vertical beam of the radar. The right-hand frame shows the corresponding profiles using the MVD-deduced vertical velocities. We see that the resulting temperatures are not very different, but the temperature gradients are greatly improved by the MVD method. We judge this by the erratic appearance of superadiabatic layers adjacent to stable layers seen in the left-hand frame, as compared with the much less noisy gradients in the right-hand frame. The five-beam system thus offers not only a substantial reduction in the noisiness of the profiles of the wind components, but a very substantial improvement in the use of RASS temperature gradients for observations of the Richardson number and turbulent length scales.

g. Length scales, fluxes, and eddy diffusion coefficients

The Richardson number is directly available from the profiler data using the temperature gradients provided

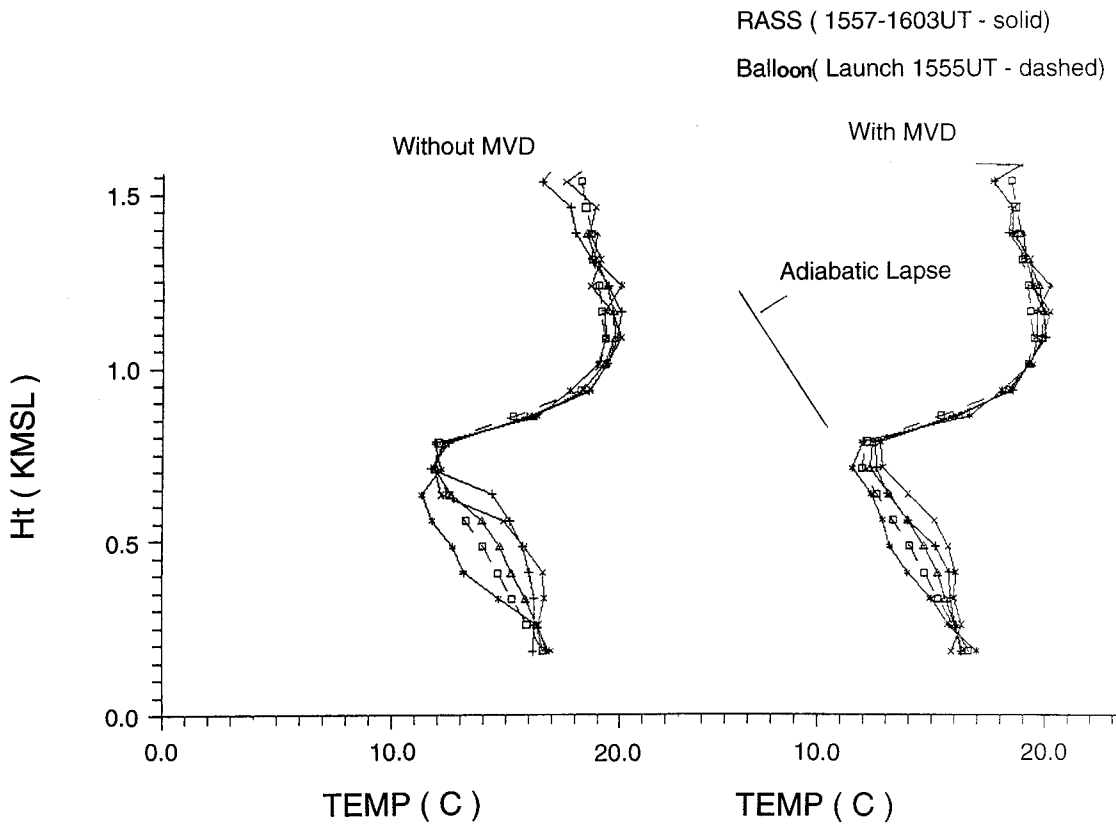

FIG. 7. Three successive RASS temperature profiles (solid) during the indicated balloon ascent (dashed). The average of the three RASS profiles is shown by the solid profile with triangles. The left frame uses the measured vertical velocity to correct the RASS temperatures. The right frame shows the same data using the vertical velocity deduced from MVD.

by the RASS system as described above, and the wind shears from the radar Doppler winds after applying the MVD technique described above. Finding ϵ from the second moment of the spectrum as described above, one kind of outer scale (L_w) and the Kolmogorov microscale are available from (2b) and (18). From the microscale, the critical smallest radar wavelength that will be unaffected by viscous damping of the turbulence beyond the inertial subrange can be found from Hill (1978) to be 8π times the microscale (Gossard et al. 1984). The scale L_w can be found from radar data alone.

Other quantities may be calculated from the radar data if collocated balloon-measured gradients are also available. For example, the length scale for potential refractive index L_ϕ may be calculated from the equation corresponding to (2a) if its height gradient is measured by balloon. It is also possible to calculate C_θ^2 and C_Q^2 from equations analogous to (2a) if the scale lengths for temperature and humidity Q are the same as L_ϕ. A Prandtl number and an eddy coefficient can also be found from (1a) and (5). The Prandtl number is really a ''pseudo'' Prandtl number whose interpretation is quasi-empirical. Its generality is constrained by the simple form of the energy and variance conservation equations used in deriving (1a) and by the homogeneity and isotropy assumptions inherent in its application.

Figures 8a–c show plots of the length scale of the vertical component of the velocity field as defined by (2b) near and within the stable layer. The solid curve is the plot of the corresponding scale for refractive index [see (2a)].

As with the Richardson number, calculation of the scales is a noisy procedure (e.g., Muschinski 1997). Because the gradients of the profiles appear squared in the denominators of (2a) and (2b), the length scales can become very large near the maxima and minima of the profiles. As noisy profiles may have many small-scale maxima and minima, the lengths vary widely. The gradients of potential functions, such as temperature and refractive index, should pass through zero only under superadiabatic conditions and conditions of positive humidity gradients. However, superadiabatic gradients are seen fairly often in the marine layer and above the dry layer capping the inversion the humidity commonly shows layers of positive gradient. Near these transitions and near the boundaries of the stable layer, the length scales can become very large (even off-scale in Figs. 8a–c), especially if the radar-measured layer boundary

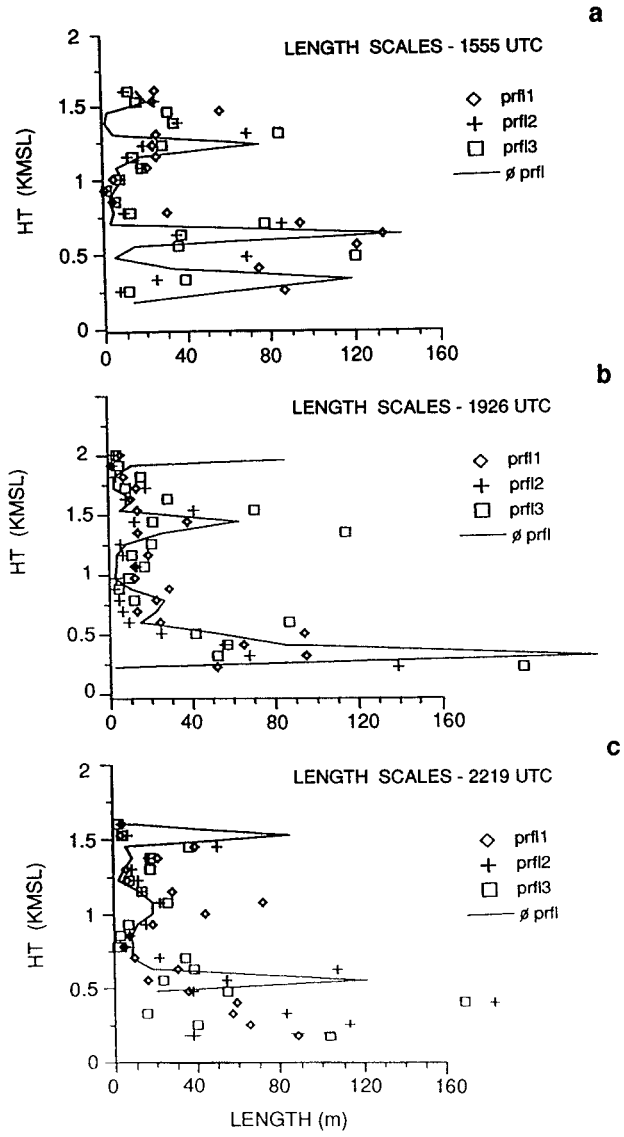

FIG. 8. Length scales calculated from (2a) and (2b) for three successive radar cycles during the three balloon soundings at (a) 1555, (b) 1926, and (c) 2219 UTC. The points are the length scale of the vertical component of velocity L_w defined by (2a). The solid curves are the length scale of ϕ multiplied by 4, calculated from the average C_ϕ^2 measured by radar and the gradient of ϕ measured by balloon, and therefore illustrate the goodness-of-fit for a ratio of 4 for the length scales. The balloon and radar inversion heights must be carefully matched. The balloon profile was raised 40 m for the 1555 and 2219 UTC profiles to match the inversion bases.

does not coincide precisely with the balloon-measured boundary. The shear can be zero only if the maxima and minima of the u and v components of the wind coincide; therefore, the velocity outer scale should very rarely pass through infinities. However, shear can become very small near speed maxima and minima, leading to occasional large spikes in the Richardson number and in the velocity outer scale.

In Figs. 8a–c, plots from the three cycles of the radar during each balloon ascent are shown as points and are to be compared with the length scale of potential refractive index (solid). A median value of the ratio L_w/L_ϕ is about 4 in these data, in contrast to the value of about 0.7 found by Gossard et al. (1984) from measurements with point sensors on a tower. Therefore, the value of L_ϕ multiplied by 4 is shown as the solid curve for comparison with L_w, and we have used this ratio in the calculations of the gradient quantities and the eddy diffusion coefficients. The problem of relating scales derived from time series recorded by point sensors to volume-integrated measurements from radar pulse volumes is reminiscent of the need for a filling factor to describe the turbulent patchiness proposed by vanZandt et al. (1978). The numerator in (3) represents a volume-averaged power density at the Bragg scale, while the denominator represents velocity variance from an integral of kinetic energy density over the whole pulse volume, assuming an inertial subrange to extend over the whole volume. If either the reflectivity in the volume is patchy or the outer scale is much less than the size of the volume, the ratio of the length scales would be increased over the point measurement, as observed. Until further comparisons with in situ measurements are available, the ratio of length scales must be considered an empirical result. The length scales show no correlation with the Richardson number, but there is clearly a strong dependence on thermal stability, which is a result also reported by Muschinski (1997) from very different measurements. Both scales are reduced to very small values within stable layers (e.g., $L_0 \simeq 3$ m in the radar cycles at about 1555 UTC, and 8 m in the 2219 UTC cycles), but there is some evidence, especially in the 1926 UTC profiles, that the ratio becomes larger than 4 within the stable zone, perhaps because of anisotropy. The corresponding eddy diffusion coefficients become very small within the upper part of the stable layer.

Figures 9a–c show averaged length scales, Prandtl number, and Richardson number from the radar data, as well as the log of the wind shear and the radar and balloon temperature profiles. The critical wavelength found from the Kolmogorov microscale [Eq. (18)] is shown in the center frame of Figs. 9a–c in centimeters. It can be as large as 20 cm within the stable zone; therefore, radars with wavelengths shorter than 40 cm can, on occasion, produce substantially less backscatter within stable layers than normally predicted from Bragg scatter theory.

Figures 10a–c show the eddy coefficients for heat and momentum (middle frames) and the corresponding fluxes of momentum (N m^{-2}) and heat (W m^{-2}) in the rightmost frames. Here, K_m was found from (5), and K_θ was found from Pr in (4), assuming $L_w/L_\phi = 4$. In calculating the momentum flux, the height gradient of wind speed was used instead of (2c). The usefulness of profilers for measuring flux remains to be established. Figures 10a–c show that the magnitudes and behavior of these quantities are qualitatively reasonable except for occasional unreasonably large spikes that occur in the neighborhood

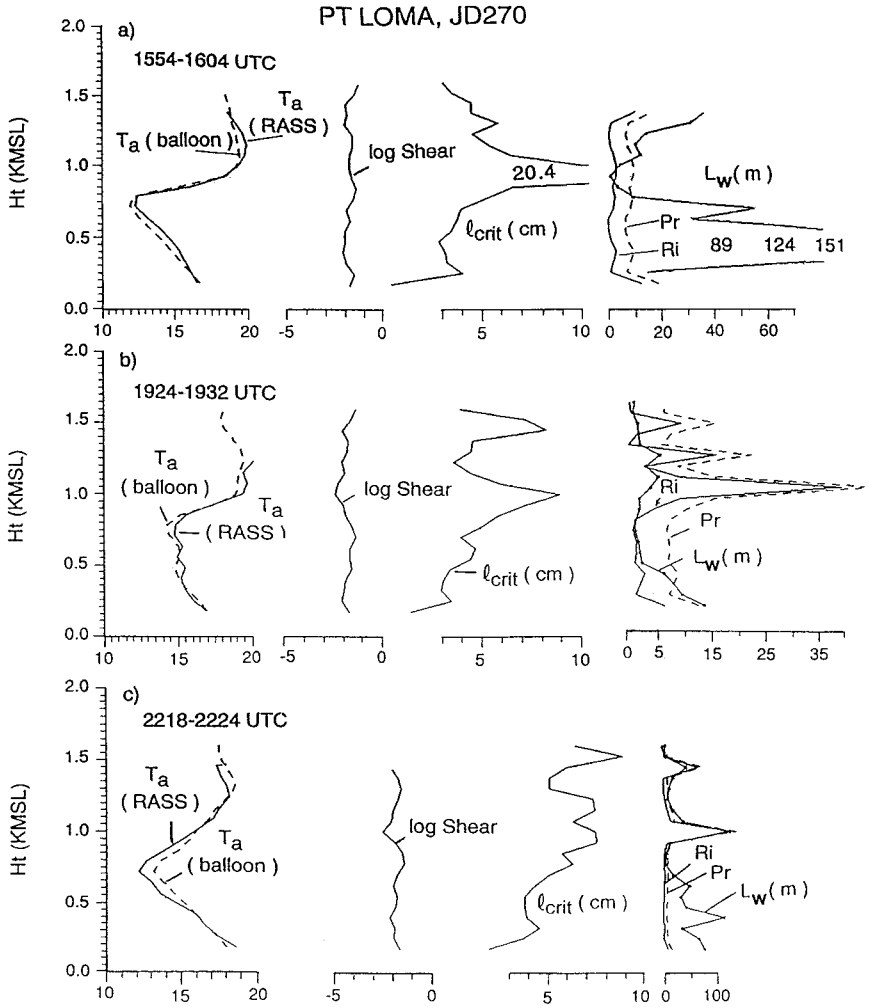

FIG. 9. Richardson number, Prandtl number, and length scales from radar data collected during the three balloon launches on 27 September 1995 (JD 270) at (a) 1555, (b) 1926, and (c) 2219 UTC. Occasionally, large spikes in Ri and L_0 occur near maxima or minima of the wind profile where shear becomes very small. Therefore, Ri and the length scales tend to be noisy. Note that the outer scale is reduced to only a few meters within the very stable zone.

of maxima and minima in the wind profiles where the shear values approach zero. The eddy coefficients are large in the marine layer, falling to very small values within the stable inversion layer. Heat fluxes are negative in the marine layer in the morning (about 0900 LT, top), becoming positive in the afternoon (about 1500 LT, bottom). These data are shown mainly to demonstrate the technique. Their quantitative accuracy remains to be established by comparison with in situ measurements because of the assumptions required in the formal development. These include the restriction of (1a) to the stable layer, the hypothesis that the ratio of length scales is approximately constant in the calculation of Pr, and the assumptions of isotropy and homogeneity even though the outer scales typically fall to less than 10 m within the inversion layers.

7. Radar sensing of the property gradients

a. Refractive-index gradients

Taking the derivative of $\underset{\sim}{\phi}$ in (6), we find the linearized equation for small perturbations to be

$$d\underset{\sim}{\phi} = \frac{\partial \underset{\sim}{\phi}}{\partial \underset{\sim}{\theta}} \partial \underset{\sim}{\theta} + \frac{\partial \underset{\sim}{\phi}}{\partial \underset{\sim}{Q}} dQ, \tag{22}$$

where

$$\frac{\partial \underset{\sim}{\phi}}{\partial \underset{\sim}{\theta}} = -\frac{77.6 p_r}{\theta_0}\left(\frac{1}{\theta_0} + 15.46\frac{Q_0}{\theta_0^2}\right) \equiv -a_0 \tag{23}$$

and

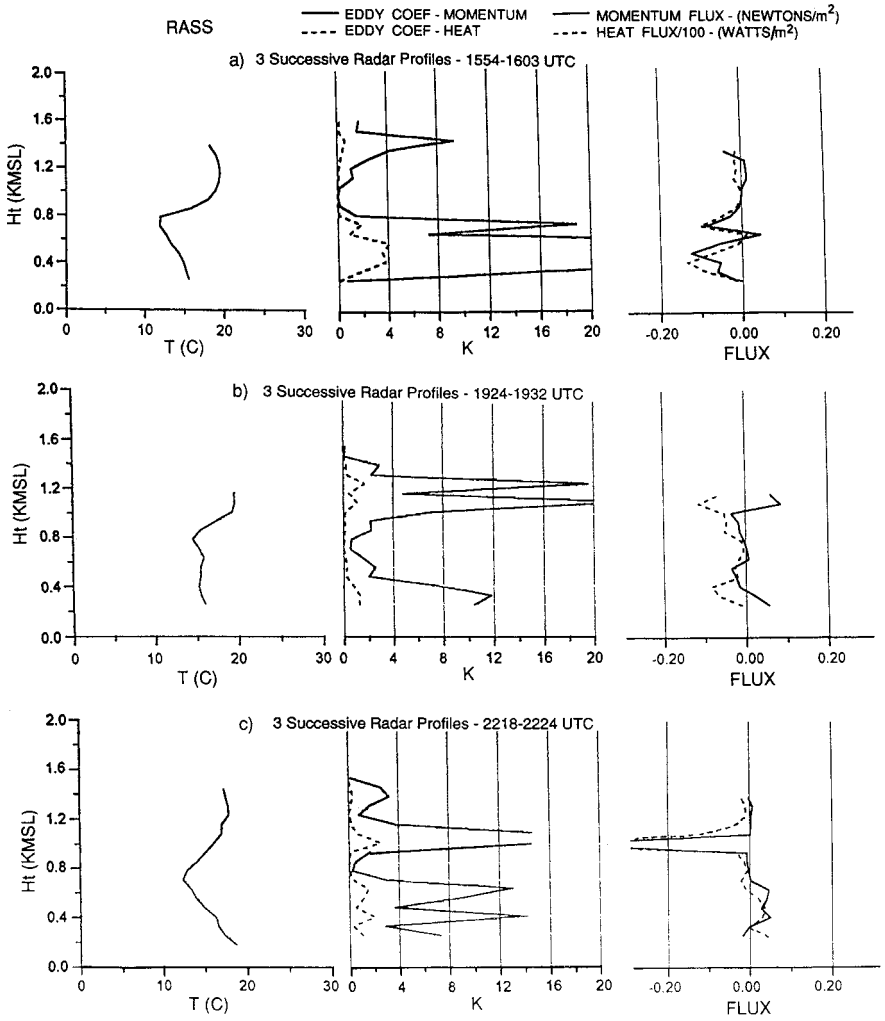

FIG. 10. Profiles of the eddy coefficients and flux computed from the radar observations, as compared with the temperature profile, measured by RASS. Units of eddy coefficient are $m^2\ s^{-1}$, and those of flux are N m^{-2} for momentum and W $m^{-2}/100$ for heat. The factor of 100^{-1} was introduced for convenience in plotting. The occasional large spike occurs near maxima and minima in the wind profiler where shear approaches zero. The time periods correspond to the balloon launch times: (a) 1555, (b) 1926, and (c) 2219 UTC.

$$\frac{\partial \phi}{\partial Q} = 77.6 p_r \left(\frac{7.73}{\theta_0^2}\right) \equiv b_0. \tag{24}$$

Thus,

$$\frac{dQ}{dz} = \left[\frac{d\phi}{dz} + a_0 \frac{d\theta}{dz}\right] b_0^{-1}. \tag{25}$$

From (25), it is clear that the gradients of humidity can be retrieved to about the same degree of accuracy as gradients of refractive index, using the temperature gradients provided by RASS. The percentage variation of the coefficients a_0 and b_0 is small in the real atmosphere. They can be fairly accurately estimated from approximations of Q_0 and θ_0 based on standard atmospheres (see Gossard et al. 1995, appendix A.3).

In accord with our earlier convention, we let $d\phi = \phi$, $d\theta = \theta$, and $dQ = Q$ so that (22) can be written as $\phi = -a_0\theta + b_0 Q$. Gossard (1960) pointed out, and Gurvich (1968) discussed, that the variance (and spectrum) of ϕ includes a temperature–humidity covariance (and cospectrum $CO_{\phi Q}$) term that can provide a large contribution (positive or negative according to the signs of the height gradients of θ_0 and Q_0) to the variance of the refractive index. The effect has more recently been shown by Friehe et al. (1975), Hill (1978), and Wyngaard et al. (1978) to be important even in calculations of optical refractive-index

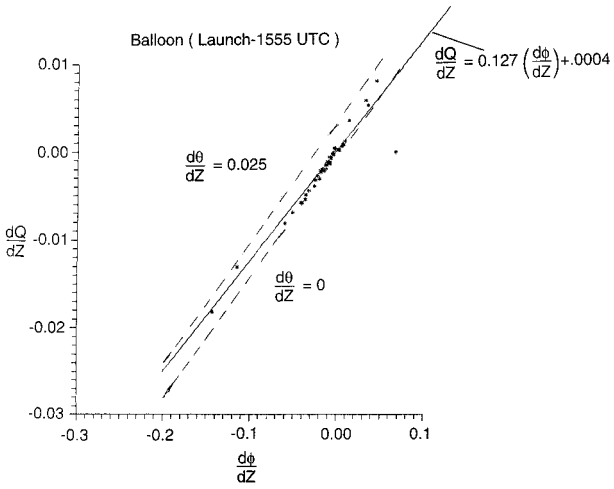

FIG. 11. Plot of refractive-index gradient vs humidity gradient from the 1555 UTC balloon launch compared with (25). This plot demonstrates that a simple linear relationship yields the humidity gradient if the refractive-index gradient is given.

perturbation parameters. Thus, the interrelationships of refractive index with temperature and humidity are

$$\overline{\phi^2} = a^2\overline{\theta^2} + b^2\overline{Q^2} - 2ab\overline{\theta Q},$$

$$C_\phi^2 = a^2C_\theta^2 + b^2C_Q^2 - 2abC_\theta C_Q,$$

and

$$S_\phi(k) = a^2S_\theta(k) + b^2S_Q(k) - 2ab\mathrm{CO}_{\theta Q}(k),$$

where CO is the cospectrum of θ and Q.

b. Humidity gradients

We note from Fig. 2b that the potential refractive-index and humidity-density profiles are virtual reproductions of each other except for scaling factors. Thus, if the radars can sense the refractive-index profile, they also provide a very accurate humidity profile. Figure 11 illustrates this quantitatively; it shows plots of (25) for an adiabatic temperature lapse rate and for a strong positive gradient of 0.025° per meter (dashed lines). As an example, we have superimposed the balloon gradient data from the 1555 UTC launch onto this plot and find very good agreement for the regression fit shown (solid line). RASS can be used to refine the contribution of the temperature gradient to the humidity calculation, but it is usually only available in the lower troposphere. Figure 11 shows that the conversion is fairly accurate even without temperature because a_0 is so much smaller than b_0; therefore, the humidity retrieval can be used to altitudes as high as accurate refractive gradients can be found.

8. Discussion of observations

It is evident from (3) that the sensing of refractive-index gradient profiles depends on accurate measurements of C_ϕ^2, C_w^2, and wind (specifically, wind shear). Figures 12a–c show these three quantities (left three frames) and the implied gradients of refractive index (right-hand frame) for the three cases intensively investigated in this paper.

The left frame of Figs. 12a–c shows the three successive profiles of log C_ϕ^2 measured by the radar during the 10 min required by the balloon to rise through the height range of usable RASS signals. As expected, the backscatter shows great enhancement in the inversion where the humidity decreases sharply. In all three time periods, C_n^2 rises to about 10^{-13} ($C_\phi^2 = 10^{-1}$) at the layer maximum. Below 400 m, in the marine layer, signals are also strong with C_n^2 reaching about 10^{-14}. It is unclear whether there is significant contribution from unwanted scatterers, such as insects moving with the air motion, low in the profile. Above 500 m, there is a zone of very weak backscatter with C_n^2 falling to about 10^{-16} in the radar soundings at around 1600 and 2220 UTC. Figure 2b shows this zone to correspond to a height range of near-adiabatic and superadiabatic lapse rates and near-zero humidity gradients.

The second frame from the left in Figs. 12a–c shows log C_w^2 derived from the second moment of the Doppler spectra (i.e., the spectral width). Most previous efforts to use spectral width to measure turbulence intensity have had only marginal success at best. Here it is evident that the resulting profiles of C_w^2 are closely related to the stably stratified zone in and above the temperature inversion. In fact, Fig. 5 shows the turbulent dissipation rate ϵ to decrease by three orders of magnitude to about 10^{-6} m^2 s^{-3} in the upper part of the inversion layer in the 1600 UTC cycles. The apparent success in the use of the second moments from the Point Loma data emphasizes the importance of editing the spectra (rather than moments of the spectra). We believe it is also important to use the regression techniques described in this paper to minimize the problems associated with contributions from overlapping spectral peaks and uncertainties about noise level.

The third frame from the left in Figs. 12a–c shows the wind speed profiles found by averaging the four sets of winds provided by each cycle of our five-beam system. At 1929 UTC, the spectra from the second cycle on the west radial, shown in the lower right frame of Fig. 4, were so ambiguous that the second wind profile was derived from only the north and east radials. The use of the MVD technique and five beams greatly improved the consistency of the shear profiles, which was very important to the calculation of outer scale and property gradients. It is evident that the wind speed profiles vary widely just below the stable layer even though the profiles are only 3.3 min apart. This is a very repeatable phenomenon and may be due in part to gravity wave perturbations. The balloon winds are not shown because this model of rawinsonde has too much temporal averaging to be of use in the radar comparison.

The right-hand frame of Figs. 12a–c shows the radar-derived gradients of refractive index compared with the

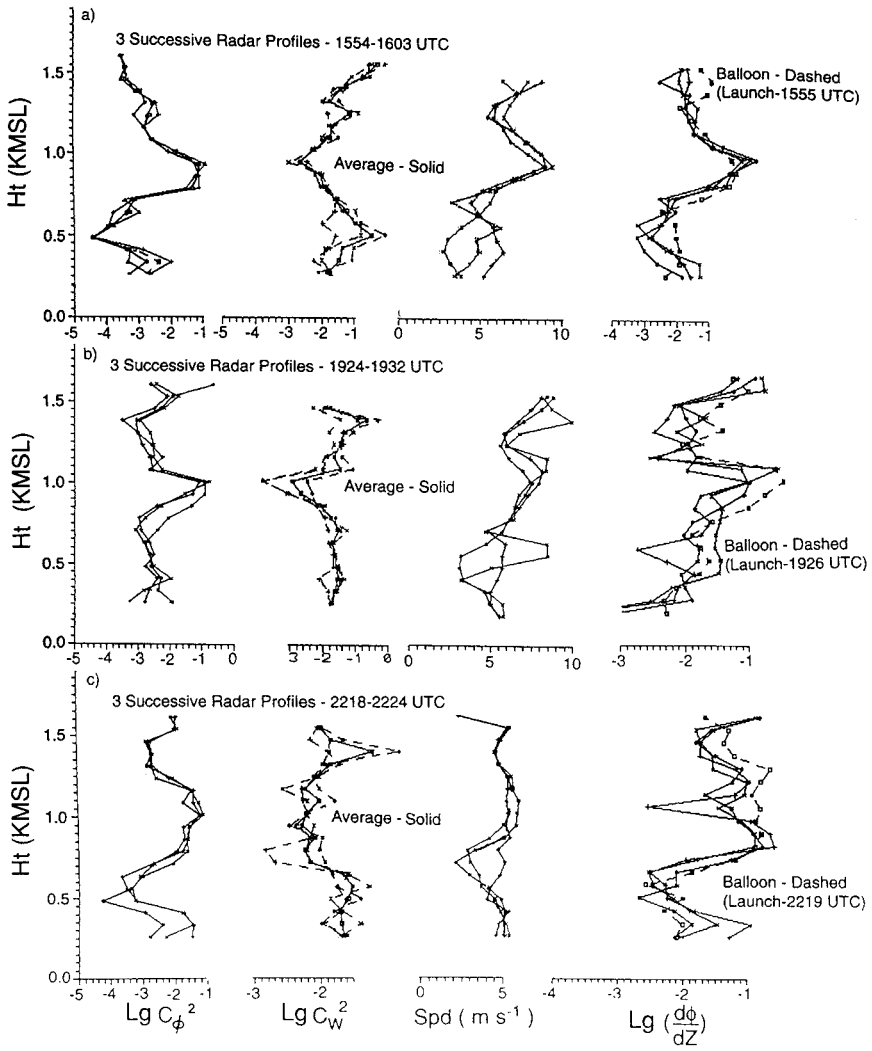

FIG. 12. Profiles of logarithms of C_ϕ^2, C_w^2, and shear (left frames) and profiles of refractive-index gradients (right frame). In the rightmost profiles, radar calculations of $d\phi/dz$ from three successive cycles during the balloon traverse are shown as solid lines; balloon data are represented by dashed squares. The time periods represented in the frames correspond to the balloon launch times: (a) 1555, (b) 1926, and (c) 2219 UTC.

balloon-measured gradients shown as the dashed profile. The agreement is satisfactory for the 1600 and 2220 UTC periods, but the radar underestimates the gradient by more than a factor of 2 in two of the three cycles in the 1930 UTC period.

The intrinsic difficulty in extracting accurate moment data from ground clutter and unwanted targets in the lower range gates probably precludes the possibility of integrating the radar gradients to obtain refractive-index profiles and may well limit the usefulness of the method to layers above the lowest few hundred meters in noisy environments. It has been suggested by Stankov et al. (1996) that the radar-measured gradients may be combined with the mathematical retrieval of humidity from radiometers or from the Global Positioning System (GPS) satellite refractive-index data to produce realistic profiles of refractive index and, therefore, humidity. The radar data would then be used to provide details of the gradient structure in the troposphere, and the satellite data would constrain the profiles to accurate totals and provide information about the upper atmosphere. The combined results for humidity would then be assimilated more or less continuously into predictive models.

Within the very stable zones of the profiles, the outer scale is reduced to only a few meters, so assumptions that the inertial subrange fills the pulse volume must be suspect in the interior of the stable layer. It is very likely that assumptions of isotropy also fail there, and such measurements are urgently needed so that error at the layer centers may be assessed.

9. Conclusions

An experiment to evaluate the capability of Doppler radar profilers to remotely measure useful meteorological quantities has been described. It is concluded that the usual wind observations obtained by editing the moments of the spectra are of marginal use unless a long-term consensus of the moments is tolerable. It is concluded that it is very important to extend the processing to include editing of the raw averaged spectra if temporal detail is important. It is also found that the redundancy of five-beam systems is very important, and a method of minimizing the variances of the differences of opposing radials is described that not only substantially improves the agreement of the redundant wind profiles but improves the vertical velocity estimate, with important consequences to the RASS temperature profiles. We conclude that acquisition of useful wind profiles is possible with spectral editing and the redundancy of a five-beam system. Otherwise, only average winds from a long-term consensus can be considered reliable.

The RASS temperature profiles provided perhaps the most impressive agreement between the balloon observations and the radar system. When corrected with the balloon-measured humidity and the vertical velocities provided by MVD, there was no discernible bias between the radar-measured and balloon-measured temperatures in the height range examined.

Another very encouraging result was the apparent accuracy of the spectral second-moment products in measuring turbulent dissipation rate and velocity structure parameters when the signal-to-noise ratio was large and when spectral editing was used. The results showed turbulence intensity to decrease by more than an order of magnitude through the inversion capping the marine layer. It was found to be very important to correct the measured second moments for antenna beamwidth and for system dwell time. Two different techniques for optimizing the calculation of spectral width are proposed. One involves integration over the uncontaminated range of the proper spectral peak and then extrapolating a Gaussian function to infinity. The other method uses the slope of the log least squares best fit of the uncontaminated points to a Gaussian function. The resulting correlation coefficient then provides a quantitative measure of the adequacy of the fit and the probable error. Further error assessment is provided by the difference in the spectral width calculated by the two methods. With the proper spectral editing and error corrections, it is concluded that the above techniques will permit the useful monitoring of turbulence intensity profiles through those height ranges of good signal-to-noise ratio. Several new processing algorithms are under development in various organizations that will help automate the techniques herein described.

The effective ratio of the length scales L_w/L_ϕ in the present data was about 4, giving $C = 6.3(du_0/dz)^2$ in (3).

The profiles of radar-measured gradients of refractive index showed satisfactory agreement with the balloon-measured gradients. However, man-generated and biological contamination low in the profile seem to preclude the possibility that accurate refractive-index profiles can be obtained by simple integration. Gradients of humidity are available to about the same accuracy as refractive-index gradients, possibly by combining the temperature gradients from RASS with the refractive-index gradient observations from the radar. However, for most purposes, the contribution of temperature is fairly unimportant in the lower atmosphere. The technique is promising for applications such as radio/radar propagation assessment, where the gradients of refractive index (or humidity) rather than their profiles are needed.

The inclusion of shear and spectral second moment improves the correlation between balloon-measured $(d\phi_0/dz)^2$ and the radar-calculated value, compared with the correlation with C_ϕ^2 alone, but only very slightly, amounting to 1% or 2% in the present data.

Acknowledgments. The authors wish to express their appreciation to R. Chadwick, D. Gottas, S. Gutman, M. J. Post, J. H. Richter, B. B. Stankov, R. G. Strauch, B. Templeman, and B. L. Weber for many helpful suggestions and encouragement. This project was partially sponsored by the Naval Command, Control and Ocean Surveillance Center and by the Office of Naval Research.

APPENDIX

A Derivation of (3) from Mixing Length Arguments

Equation (1a) is derived for turbulent perturbations under stable conditions using the turbulent energy balance equation and the variance conservation equation. Some flux terms for pressure perturbations and higher-order perturbation products are neglected. We now derive it in a way that provides different conceptual insight into the physics and the nature of the assumptions, especially the role of isotropy.

The concept of properties being mixed in mean gradients is illustrated schematically in Fig. A1, where (mixing) length scales ℓ_v and ℓ_ϕ are defined for velocity and for a passive scalar, respectively. If local isotropy is assumed, $\overline{u'^2} = \overline{v'^2} = \overline{w'^2}$, so, choosing w,

$$\overline{w'^2} = \ell_v^2\left(\frac{du_0}{\partial z}\right)^2 \tag{A1}$$

and

$$\overline{\phi'^2} = \ell_\phi^2\left(\frac{d\phi_0}{\partial z}\right)^2. \tag{A2}$$

The variance contributed by the inertial subrange of turbulence is given by

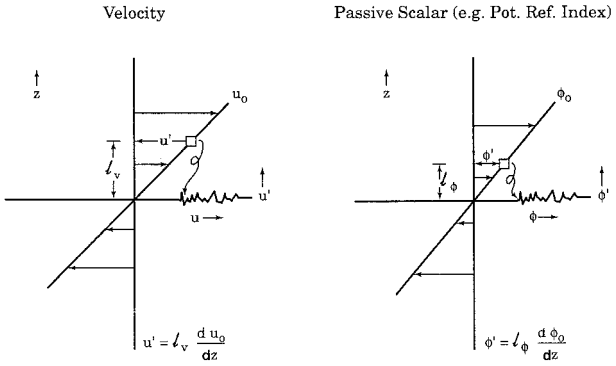

FIG. A1. Schematic picture of a mixing length concept that leads to an equation in the same form as (3), which was derived from the energy equation and variance balance equations.

$$\overline{w'^2} = \int_{k_0}^{\infty} S_w(k)\, dk = 0.25 C_w^2 \int_{k_0}^{\infty} k^{-5/3}\, dk$$
$$= (1/6)(2\pi)^{-2/3} C_w^2 L_w^{2/3} \quad \text{(A3)}$$

and

$$\overline{\phi'^2} = \int_{k_1}^{\infty} S_\phi(k)\, dk = 0.25 C_\phi^2 \int_{k_1}^{\infty} k^{-5/3}\, dk$$
$$= (1/6)(2\pi)^{-2/3} C_\phi^2 L_\phi^{2/3}, \quad \text{(A4)}$$

where $k_0 = 2\pi/L_v$ and $k_1 = 2\pi/L_\phi$, and $S_w(k)$ and $S_\phi(k)$ are the spectra of w and ϕ, respectively, in the inertial subrange. The factor 0.25 is a ratio of Kolmogorov constants. For large-scale mixing, the variance is dominated by the gradient mixing represented by (A1) and (A2); for the smaller scales, the variance contributed by the (assumed isotropic) mixing in the inertial subrange dominates. The scales at which the contributions are just equal defines L_w and L_ϕ (e.g., Tatarskii 1971, 72), so that

$$\frac{\left(\frac{\partial u_0}{\partial z}\right)^2}{\left(\frac{\partial \phi_0}{\partial z}\right)^2} = \frac{C_w^2 L_w^{-4/3}}{C_\phi^2 L_\phi^{-4/3}}, \quad \text{(A5)}$$

which yields (3). A major goal of this paper has been to examine the ratio of L_w and L_ϕ under a wide range of stability conditions.

REFERENCES

Andreas, E. L., 1987: On the Kolmogorov constants for the temperature-humidity co-spectrum and the refractive-index spectrum. *J. Atmos. Sci.,* **44,** 2399–2406.

Atlas, D., 1964: Advances in radar meteorology. *Advances in Geophysics,* Vol. 10, Academic Press, 317–478.

——, K. Hardy, K. M. Glover, I. Katz, and T. G. Konrad, 1966: Tropopause detected by radar. *Science,* **153,** 1110–1112.

Batchelor, G. K., 1953: *The Theory of Homogeneous Turbulence.* Cambridge University Press, 195 pp.

Battan, L. J., 1973: *Radar Observation of the Atmosphere.* University of Chicago Press, 323 pp.

Bean, B. R., and E. J. Dutton, 1966: *Radio Meteorology.* Monograph No. 92, National Bureau of Standards, 431 pp.

Chadwick, R. B., and E. E. Gossard, 1983: Radar remote sensing of the clear atmosphere—Review and applications. *Proc. IEEE,* **71,** 738–753.

Cohn, S. A., 1995: Radar measurements of turbulent eddy dissipation rate in the troposphere: A comparison of techniques. *J. Atmos. Oceanic Technol.,* **12,** 85–95.

Corrsin, S., 1951: On the presence of isotropic temperature fluctuations in isotropic turbulence. *J. Appl. Phys.,* **22,** 417–423.

Doviak, R. J., and D. S. Zrnić, 1984: *Doppler Radar and Weather Observations.* Academic Press, 458 pp.

Friehe, C. A., J. C. LaRue, F. H. Champagne, C. H. Gibson, and G. F. Dreyer, 1975: Effects of temperature and humidity fluctuations on the optical refractive index in the marine boundary layer. *J. Opt. Soc. Amer.,* **65,** 1502–1511.

Friend, A. W., 1949: Theory and practice of tropospheric sounding by radar. *Proc. IEEE,* **37,** 116–138.

Frisch, A. S., and S. F. Clifford, 1974: A study of convection capped by a stable layer using Doppler radar and acoustic echo sounders. *J. Atmos. Sci.,* **31,** 1622–1628.

Fukao, S., and Coauthors, 1994: Seasonal variability of vertical eddy diffusivity in the middle atmosphere. *J. Geophys. Res.,* **99,** 18 973–18 987.

Gage, K. S., J. L. Green, and T. E. vanZandt, 1980: Use of Doppler radar for the observation of atmospheric turbulence parameters from the intensity of clear air echoes. *Radio Sci.,* **15,** 407–416.

Gorelik, A. G., and Y. V. Mel'nichuk, 1963: Radar study of dynamic processes in the atmosphere. *Tr. Vses. Nav. Meteor. Souesh.,* **5,** 33–42.

Gossard, E. E., 1960: Power spectra of temperature, humidity, and refractive index from aircraft and tethered balloon measurements. *IEEE Trans. Antennas Propag.,* **AP-8,** 186–201.

——, 1990: Radar research on the atmospheric boundary layer. *Radar in Meteorology,* D. Atlas, Ed., Amer. Meteor. Soc., 477–527.

——, and R. G. Strauch, 1983: *Radar Observations of Clear Air and Clouds.* Elsevier, 280 pp.

——, and A. S. Frisch, 1987: Relationship of the variances of temperature and velocity to atmospheric static stability—Application to radar and acoustic sounding. *J. Climate Appl. Meteor.,* **26,** 1021–1036.

——, and N. Sengupta, 1988: Measuring gradients of meteorological properties in elevated layers with a surface-based Doppler radar. *Radio Sci.,* **23,** 625–693.

——, J. H. Richter, and D. Atlas, 1970: Internal waves in the atmosphere from high-resolution radar measurements. *J. Geophys. Res.,* **75,** 903–913.

——, R. B. Chadwick, W. D. Neff, and K. P. Moran, 1982: The use of ground-based Doppler radars to measure gradients, fluxes, and structure parameters in elevated layers. *J. Appl. Meteor.,* **21,** 211–226.

——, ——, R. T. Detman, and J. Gaynor, 1984: Capability of surface-based, clear-air Doppler radar for monitoring meteorological structure of elevated layers. *J. Climate Appl. Meteor.,* **23,** 474–490.

——, D. C. Welsh, and R. G. Strauch, 1990: Radar-measured height profiles of C_n^2 and turbulence dissipation rate compared with radiosonde data during October 1989 at Denver. NOAA TR ERL 442-WPL 63, Environmental Technology Laboratory, Boulder, CO, 115 pp. [Available from the National Technical Information Service, 5285 Port Royal Rd., Springfield, VA 22161.]

——, R. G. Strauch, B. B. Stankov, and D. E. Wolfe, 1995: Measurement of property gradients and turbulence aloft with ground-based Doppler radars. NOAA TM ERL 453-ETL 67, Environmental Technology Laboratory, Boulder, CO, 31 pp. [Available from the National Technical Information Service, 5285 Port Royal Rd., Springfield, VA 22161.]

——, J. B. Snider, E. E. Clothiaux, B. Martner, J. S. Gibson, R. A. Kropfli, and A. S. Frisch, 1997: The potential of 8-mm radars for

remotely sensing cloud drop size distributions. *J. Atmos. Oceanic Technol.,* **14,** 201–228.

Gurvich, A. S., 1968: Effect of absorption on the fluctuation in signal level during atmospheric propagation. *Radio Eng. Electron. Phys.,* **13,** 1687–1694.

Hill, R. J., 1978: Models of the scalar spectrum for turbulent advection. *J. Fluid Mech.,* **88,** 541–562.

——, 1989: The structure functions and spectra of scalar quantities in the inertial convective and viscous convective ranges of turbulence. *J. Atmos. Sci.,* **46,** 2245–2251.

Hocking, W. K., 1983: On the extraction of atmospheric turbulence parameters from radar backscatter Doppler spectra: I. Theory. *J. Atmos. Terr. Phys.,* **45,** 89–102.

——, 1995: An assessment of the capabilities and limitations of radars in measurements of upper atmosphere turbulence. *Adv. Space Res.,* **17** (11), 37–47.

Katz, I., 1951: *The Propagation of Short Radio Waves.* McGraw-Hill Book Co., 199 pp.

Kondo, J., O. Kanechika, and N. Yasuda, 1978: Heat and momentum transfers under strong stability in the atmospheric turbulent layer. *J. Atmos. Sci.,* **35,** 1012–1021.

Labbitt, M., 1981: Coordinated radar and aircraft observations of turbulence. Rep. ATC-108, MIT Lincoln Laboratory, Lexington, MA, 40 pp.

Lumley, J. L., and H. A. Panofsky, 1964: *The Structure of Atmospheric Turbulence.* Wiley, 239 pp.

May, P. T., K. P. Moran, and R. G. Strauch, 1989: The accuracy of RASS temperature measurements. *J. Appl. Meteor.,* **28,** 1329–1335.

Muschinski, A., 1997: Turbulence and gravity waves in the vicinity of a midtropospheric warm front: A case study using VHF echo-intensity measurements and radiosonde data. *Radio Sci.,* **32,** 1161–1178.

Nastrom, G. D., 1997: Doppler radar spectral width broadening due to beamwidth and wind shear. *Ann. Geophys.,* **15,** 786–796.

——, and F. D. Eaton, 1997: A brief climatology of eddy diffusivities over White Sands Missile Range, New Mexico. *J. Geophys. Res.,* **102,** 29 819–29 826.

Ottersten, H., 1969: Atmospheric structure and radar backscattering in clear air. *Radio Sci.,* **4,** 1179–1193.

Peters, G. H., H. Timmerman, and H. Hinzpeter, 1983: Temperature sounding in the planetary boundary layer by RASS—System analysis and results. *Int. J. Remote Sens.,* **4,** 49–63.

Priestley, J. T., and R. J. Hill, 1985: Measuring high-frequency humidity, temperature, and radio refractive index in the surface layer. *J. Atmos. Oceanic Technol.,* **2,** 233–251.

Richter, J. H., 1969: High-resolution tropospheric radar sounding. *Radio Sci.,* **4,** 1261–1268.

Saxton, J. A., S. A. Lane, and R. W. Meadows, 1964: Layer structure of the troposphere-simultaneous radar and microwave refractometer investigations. *Proc. IEEE London,* **3,** 275–283.

Sirmans, D., and R. J. Doviak, 1973: Meteorological radar signal intensity estimation. NOAA TM ERL NSSL-64, 80 pp. [Available from the National Technical Information Service, 5285 Port Royal Rd., Springfield, VA 22161.]

Srivastava, R. C., and S. D. Atlas, 1972: The effects of a finite radar pulse volume on turbulence measurements. Preprints, *15th Radar Meteorology Conf.,* Urbana, IL, Amer. Meteor. Soc., 297–302.

Stankov, B. B., E. R. Westwater, and E. E. Gossard, 1996: Use of wind profiler estimates of significant moisture gradients to improve humidity profile retrieval. *J. Atmos. Oceanic Technol.,* **13,** 1285–1290.

Strauch, R. G., and F. H. Merrem, 1976: Structure of an evolving hailstorm. Part III: Internal structure from Doppler radar. *Mon. Wea. Rev.,* **104,** 588–595.

——, D. A. Merritt, K. P. Moran, K. B. Earnshaw, and D. van de Kamp, 1984: The Colorado wind-profiling network. *J. Atmos. Oceanic Technol.,* **1,** 37–49.

Tatarskii, V. I., 1971: The effects of the turbulent atmosphere on wave propagation. Israel Program for Scientific Translations, Jerusalem, NTIS TT 68-50464, 472 pp. [Available from the National Technical Information Service, 5285 Port Royal Rd., Springfield, VA 22161.]

vanZandt, T. E., J. L. Green, K. S. Gage, and W. L. Clark, 1978: Vertical profiles of refractivity turbulence structure constant: Comparison of observations by the Sunset radar with a new theoretical model. *Radio Sci.,* **13,** 819–829.

Warnock, J. M., and T. E. vanZandt, 1985: A statistical model to estimate the refractivity turbulence structure constant C_n^2 in the free atmosphere. NOAA TM ERL AL-10, NOAA Environmental Research Laboratories, Boulder, CO, 175 pp.

Wyngaard, J. C., W. T. Pennell, D. H. Lenschow, and M. A. LeMone, 1978: The temperature-humidity covariance budget in the convective boundary layer. *J. Atmos. Sci.,* **35,** 48–58.